Reducing the Effects of Weak Homonuclear Dipolar Coupling with CPMG Pulse Sequences for Static and Spinning Solids

Adam R. Altenhof[1,2], Zhehong Gan[2], and Robert W. Schurko[1,2,*]

1. Department of Chemistry and Biochemistry, Florida State University, Tallahassee, FL 32306, USA

2. National High Magnetic Field Laboratory, 1800 East Paul Dirac Drive, Tallahassee, FL 32310, USA

*Author to whom correspondence should be addressed.

E-mail: rschurko@fsu.edu

Tel: (850)-645-8614

Abstract

The Carr-Purcell/Meiboom-Gill (CPMG) pulse sequence, initially introduced for measuring transverse relaxation time constants (T_2), can provide significant signal enhancements for solid-state NMR (SSNMR) spectra. The proper implementation of CPMG for acquiring spectra influenced by chemical shift anisotropies (CSAs), first and/or second order quadrupolar interactions, or paramagnetic broadening has been well documented to date, as have the effects of heteronuclear dipolar coupling on CPMG echo trains and T_2 lifetimes. Homonuclear dipolar coupling can also impact T_2 lifetimes and CPMG echo trains; these effects have been thoroughly investigated for spectra of homonuclear dipolar coupled spin-1/2 nuclei typically acquired under static conditions that are predominantly influenced by dipolar broadening (*e.g.*, ^{1}H, ^{19}F, *etc*.). In particular, it has been shown that short refocusing pulses with small flip angles can extend the effective T_2 (T_2^{eff}, the observed T_2 constant as impacted by experimental conditions) measured by CPMG sequences for strong homonuclear dipolar coupled spin-1/2 pairs under static conditions. To date, these effects have not been explored for (i) spin-1/2 nuclei that have significant CSAs and simultaneously feature weak homonuclear dipolar couplings, (ii) for quadrupolar nuclei that are also weakly homonuclear dipolar coupled, and (iii) for either of these cases under magic-angle spinning (MAS) conditions. Herein, we demonstrate that short refocusing pulses that cause small flip angles can reduce the attenuation of signal in CPMG echo trains resulting from dipolar dephasing caused by the weak homonuclear dipolar couplings. For both spin-1/2 and quadrupolar nuclei, this can lead to significant extensions in T_2^{eff} and signal enhancements of up to three times compared to conventional CPMG in favourable cases. These phenomena can occur under both static and magic-angle spinning (MAS) conditions, in the latter of which homonuclear couplings are reintroduced by rotational resonance (R^2) recoupling. Experimental examples of ^{13}C ($I = 1/2$), ^{2}H ($I = 1$), ^{87}Rb ($I = 3/2$), ^{23}Na ($I = 3/2$), and ^{35}Cl ($I = 3/2$) NMR under static and MAS conditions, as well as simulations of these phenomena, are shown and discussed.

Keywords: Solid-state NMR spectroscopy; CPMG; Homonuclear Dipolar Coupling; Rotational Resonance; Signal Enhancement

1. Introduction

The Carr-Purcell/Meiboom-Gill (CPMG) pulse sequence was introduced for measuring transverse relaxation time constants (T_2),[1,2] and variants were later adapted for enhancing signal-to-noise ratios (SNR) in SSNMR experiments by Slichter and co-workers, who used these to acquire ^{17}O, ^{89}Y, and ^{13}C SSNMR spectra.[3–5] The appropriate implementation of CPMG sequences for SNR enhancement was later found to depend on which NMR interaction(s) is(are) dominant in a given spin system, including the chemical shift anisotropy (CSA), the first- and/or second-order quadrupolar interactions (FOQI/SOQI), paramagnetic interactions, dipolar interactions, and any combination thereof. For instance, Bloom and Sternin, followed by Larsen and coworkers, developed the quadrupolar (Q)CPMG pulse sequence for efficient acquisition of SSNMR spectra of integer- and half-integer-spin nuclei,[6–9] the practical aspects of which are nicely detailed by Hung and Gan (particularly for wideline spectra).[10] Iijima and coworkers have demonstrated the use of a modified (Q)CPMG sequence for acquiring paramagnetically broadened ^{2}H spectra.[11,12] Further explorations in this vein include those of O'Dell, Schurko, and co-workers, who introduced the WURST-CPMG pulse sequence for the efficient acquisition of wideline and ultra-wideline NMR spectra of both spin-1/2 and quadrupolar nuclei.[13–16] More recently, Grandinetti and coworkers demonstrated augmenting the *effective* T_2's (T_2^{eff}, *vide infra*) of central transition (CT, $+1/2 \leftrightarrow -1/2$) powder patterns of half-integer spin quadrupolar nuclei by weak RF irradiation with CPMG.[17]

Direct dipolar interactions can significantly impact the implementation and performance of the CPMG pulse sequence. This impact can be determined from quantities that arise intrinsically from relaxation, such as the transverse relaxation time constant, T_2. The effective T_2 (T_2^{eff}) measured by CPMG sequences can also be impacted, which differs from the natural T_2

based on experimental conditions (*e.g.*, decoupling, finite pulse effects and imperfections, echo spacings, temperature effects, MAS,[18] magic-angle offsets, *etc*.). Moreover, there are phenomena that affect the broadening of spectral lines or powder patterns that also influence CPMG acquisitions that arise from wholly secular, non-relaxative effects, such as inhomogeneous broadening resulting from anisotropic NMR interactions and magnetic susceptibilities; these are generally classified as T_2^* effects, or effective T_2^* ($T_2^{*\text{eff}}$) effects, which can differ from T_2* effects, depending upon the experimental conditions (*e.g.,* field inhomogeneities, decoupling, MAS, *etc*.). Heteronuclear (*IS*) dipolar interactions (where *I* and *S* are the abundant and dilute nuclei, respectively) are known to impact both T_2^* and T_2, the latter of which can reduce the number of spin echoes acquired in a CPMG echo train if there are significant contributions from heteronuclear dipolar relaxation mechanisms.[19,20] Heteronuclear dipolar decoupling is therefore often implemented with CPMG to minimize these contributions, thereby extending the T_2^{eff} to allow for acquisitions of higher SNR spectra.[16,21–23] It has similarly been observed that homonuclear (*II* or *SS*) dipolar interactions can influence the T_2 behaviour observed with Hahn echo, CPMG, and other multiple-pulse sequences. These effects depend on homonuclear dipolar coupling being in the strong or weak regime, as defined by the chemical shift difference between the coupled spins being less or greater than the orientation-dependent dipolar coupling strength, respectively (*i.e.*, $\Delta\nu_{\text{iso}} \lesssim \nu_{\text{D}}$ or $\Delta\nu_{\text{iso}} \gg \nu_{\text{D}}$, respectively). For instance, it has been demonstrated that strong homonuclear dipolar decoupling can impact T_2^{eff} and $T_2^{*\text{eff}}$ under static and MAS conditions with pulse sequences such as with WAHUHA, Lee Goldberg (LG) irradiation, DUMBO, and others.[24–27] It has also been demonstrated that Carr-Purcell or CPMG pulse sequences that use short $\theta_{\text{ref}} = 90°$ pulses, and more generally, arbitrarily small refocusing pulse flip angles, can extend T_2^{eff} for spin-1/2 nuclei that experience strong homonuclear dipolar

couplings.[28–30] Depending on the flip angle and echo spacing, the T_2^{eff} can be increased to a limit that approaches $T_{1\rho}$.[31–34] Siegel *et al*. demonstrated drastic signal enhancements in wideline spin-1/2 spectra acquired with CPMG using 90° refocusing pulses, which in part was accredited to reducing the effects of homonuclear dipolar coupling.[21,35] To date, the effects of weak homonuclear dipolar coupling in CPMG echo trains with short refocusing pulses has not been investigated for quadrupolar nuclei under static or MAS conditions..

MAS can average or remove the manifestation of the anisotropic broadening encoded by various NMR interactions such as CSA and dipolar coupling for achieving high spectral resolution. However, for homonuclear dipolar coupled spins, dipolar interactions can be reintroduced under certain conditions known as rotational resonance (R^2),[36–40] where the spinning rate, ν_{rot}, matches an integer multiple of the isotropic shift difference between a spin pair as $\Delta\nu_{iso} = n\nu_{rot}$. Primary R^2 conditions occur for n = 1,2; higher-order n = 0 and $n > 2$ conditions can occur in the presence of CSA and quadrupolar interactions. For small molecules, the n = 0 R^2 recoupling condition usually occurs between the spins of the same atomic site of neighboring molecules.[41,42] The following studies outline important examples and first discoveries of such conditions. Gan and Robyr have described the spin diffusion for spin-1 ^{2}H nuclei enhanced by the n = 0 R^2 recoupling.[43] Kwak *et al.* have described the n = 0 R^2 phenomenon that can occur between the CT and ST for half-integer spin nuclei. The recoupling to the ST is highly sensitive to the magic-angle setting which induces intriguing magic-angle effects on the T_1 measured by inversion recovery and the measured T_2^{eff}.[44,45] Finally, Edén and Frydman have also detailed R^2 mechanisms for half-integer spin quadrupolar nuclei.[40,46]

Herein, we discuss the impact of weak homonuclear dipolar couplings on the T_2^{eff}-weighted decay of CPMG echo trains and concomitant spectra acquired with CPMG pulse

sequences for spin-1/2 and quadrupolar nuclei. This weak homonuclear coupling effect is often significant for small molecules with abundant high-γ nuclei; however, some other cases with moderate abundances and/or moderate-to-low values of γ are also explored. It is shown that short refocusing pulses can reduce the effects of the homonuclear dipolar interaction on the echo train and make the T_2^{eff} longer, which leads to an overall signal enhancement in the resulting NMR spectra (this effect occurs to a degree outweighing the reduced efficiencies of shorter refocusing pulses). Several experimental examples are showcased, including ^{13}C ($I = 1/2$), ^{2}H ($I = 1$), ^{87}Rb ($I = 3/2$), ^{23}Na ($I = 3/2$), and ^{35}Cl ($I = 3/2$) NMR under static and MAS conditions. Numerical simulations of model spin systems provide insight to the underlying mechanisms and spin dynamics.

2. Experimental

2.1 Samples

Partially-deuterated α-glycine [α-glycine-d_2, Cambridge Isotope Laboratories, Inc.], urea-d_4 [Sigma Aldrich], 1,8-dimethylnapthelene-d_{12} [Cambridge Isotope Laboratories, Inc.], 1,2-phthalic anhydride-$^{13}C_2$ [Sigma Aldrich], rubidium nitrate [$RbNO_3$, Sigma Aldrich], sodium sulfate [Na_2SO_4, Sigma Aldrich], L-histidine hydrochloride monohydrate [L-Histidine HCl·H_2O, MP Biomedicals, LLC] were purchased, and deuterated MIL-53(Al)-d_4 was synthesized according to the literature.[47,48] Benzoic acid and dimedone were purchased and then deuterated by ball milling with D_2O to produce benzoic acid-*d* and dimedone-*d*, respectively. The identities and purities of the samples were verified through comparisons with previously reported NMR spectra and PXRD patterns.[48,49] All samples were ground into fine powders and packed into 3.2 mm rotors or 5 mm outer-diameter glass tubes that were sealed with Teflon tape.

2.2 Solid-State NMR Spectroscopy

NMR spectra were acquired using a Bruker Avance NEO console and a 14.1 T Magnex/Bruker ($\upsilon_0(^1H)$ = 600 MHz) wide-bore magnet at resonance frequencies of $\upsilon_0(^2H)$ = 92.104 MHz, $\upsilon_0(^{23}Na)$ = 158.730 MHz, $\upsilon_0(^{35}Cl)$ = 58.792 MHz, and $\upsilon_0(^{87}Rb)$ = 196.348 MHz, and using a Bruker Avance NEO console with a 18.8 T Oxford ($\upsilon_0(^1H)$ = 800 MHz) medium-bore magnet at a resonance frequency $\upsilon_0(^{13}C)$ = 201.096 MHz. A home-built 5 mm double-resonance (HX) static probe was used for static ^2H and ^{35}Cl experiments at 14.1 T, a home-built 3.2 mm triple resonance (HXY) magic-angle spinning (MAS) probe was used for ^{23}Na and ^{87}Rb experiments at 14.1 T, and a home-built 3.2 mm HXY MAS probe was used for ^1H-^{13}C experiments at 18.8 T. Spectra were acquired with ^1H continuous-wave (CW) decoupling with RF fields of 50 kHz for compounds having protons. RF pulse powers and chemical-shift reference frequencies were calibrated using the following standards: ^2H reference: D_2O (*l*) with δ_{iso} = 4.8 ppm; ^{13}C reference: ^{13}C-glycine (*s*) with δ_{iso} = 176.5 ppm; ^{35}Cl reference: NaCl (s) with δ_{iso} = 0.0 ppm; and the following were only used as chemical-shift references: ^{87}Rb reference: 0.1 M RbCl in D_2O (*aq*) with δ_{iso} = 0.0 ppm; ^{23}Na reference: 0.1 M NaCl in D_2O (*aq*) with δ_{iso} = 0.0 ppm. ^{23}Na and ^{87}Rb RF pulse powers were calibrated by finding the main spin-lock rotary resonance conditions, $(S+1/2)\nu_1 = \nu_{rot}$,[50,51] at ν_{rot} = 5 kHz and 10 kHz with Na_2SO_4 and $RbNO_3$, respectively.

2.3 Simulations

All numerical spin-density matrix simulations were conducted in SIMPSON 4.2.1 using either 4180 or 28656 orientations sampled according to the ZCW averaging scheme.[52,53]

Simulations with dipolar couplings use two spins with a single dipolar coupling between them. CPMG pulse sequences are simulated using 32 spin echoes in all cases. All calculations were performed on a PC operating with Windows 10 using an Intel i9-9920X CPU.

3. Results and Discussion

3.1 Pulse Sequence Considerations and Overview

The optimal implementations of the spin-echo and/or CPMG pulse sequences depend on what NMR interactions are dominant in the observed system. The sequence is typically initiated with an excitation pulse with a flip angle $\theta_{exc} = 360\nu_1\tau_{exc}$ (in degrees) of 90° (in the case of half-integer quadrupolar nuclei, a CT-selective excitation pulse is used, $\theta_{exc}^{sel} = \theta_{exc}/(I + 1/2)$).[54,55] The refocusing pulse has a flip angle, θ_{ref}, that depends upon which NMR interactions are being refocused (**Figure S1**, N.B.: the same refocusing pulse is used repeatedly within the CPMG train). For spin interactions with a linear operator of the observed spin [*e.g.,* CSA, paramagnetic broadening, and/or SOQI (when $\nu_Q \gg \nu_1$)], $\theta_{ref} = 180°$ (or CT selective, $\theta_{ref}^{sel} = 180°/(I + 1/2)$) optimally refocuses the evolution of the isochromats evolving under these interactions to form the spin echo (this is most commonly referred to as the Hahn-echo pulse sequence). For spin interaction with traceless bilinear spin operators (*e.g.,* homonuclear dipole-dipole and FOQI), $\theta_{ref} = 90°$ is optimal; these are often referred to as a solid- and quadrupolar-echo sequences, respectively. For simplicity, θ is used herein to refer to the refocusing pulse flip angle, unless otherwise stated. In the above cases, if a small θ (*i.e.* $\theta < 180°$ or $< 90°$ for linear or bilinear interactions, respectively) is used, it generates an effective rotation axis ($B_{1,eff}$) that deviates from the direction of B_1 for the refocusing of spin polarization, resulting in a reduced projection of spin polarization in the *xy*-plane of the rotating frame.[56,57] If these small θ refocusing pulses are

used, by shortening the pulse width and fixing the RF amplitude, that results in reduced signal intensity, but has the added benefit of increased refocusing bandwidth, which is useful for wideline or ultra-wideline systems.[10,58] The total sensitivity gain afforded from CPMG also strongly depends on the decay of the echo train (*i,e.* T_2^{eff}), where long T_2^{eff}'s allow for the acquisition of many spin echoes, resulting in increased SNR. In this study, we will show that for various spin systems with weak homonuclear dipolar couplings that CPMG pulse sequences using small-θ refocusing pulses can prolong the decay of the echo-train (*i.e.*, increased T_2^{eff}). The signal gain from increased T_2^{eff} can often outweigh the reduction in signal arising from decreased pulse sequence efficiency, resulting in an enhancement of overall SNR for CPMG spectra.

We will consider homonuclear dipolar coupling in two regimes: strong coupling and weak coupling, which are defined as cases where the shift differences between coupled spins are smaller or larger than the dipolar coupling strength, respectively. For strong homonuclear dipolar coupling, such as that between protons in diamagnetic solids, the chemical shift differences are almost always much smaller than typical ^{1}H-^{1}H dipolar couplings. The terms of the homonuclear dipolar Hamiltonian that yield secular effects in spectra include the dipolar order ($S_{jz}S_{kz}$) and flip-flop ($S_{j+}S_{k-} + S_{j-}S_{k+}$) terms, which are written together as $3S_{jz}S_{kz} - (S_{jx}S_{kx} + S_{jy}S_{ky})$ (where j and k are the unique spin labels). 90° excitation and refocusing pulses effectively toggle the rotating frames in the spin-space among the *x*-, *y*-, and *z*-axes. The toggling frames effectively average the effects of the homonuclear dipolar Hamiltonian, achieving the well-known solid-echo and homonuclear dipolar decoupling.[24,59,60] Similar solid echoes can be obtained in CPMG sequences employing 90° refocusing pulses; however, these echoes usually decay very quickly, especially for cases of narrow peaks/patterns, which require long echo windows. Usually, refocusing pulses used with very short echo windows are referred to as pulsed spin-lock sequences instead of

CPMG.[61,62] For this reason, we do not consider the case of strong dipolar coupling herein (*e.g.*, large ^{1}H-^{1}H couplings in diamagnetic solids). The homonuclear dipolar interactions considered in this work are in the weak coupling regime. Hence, the flip-flop terms can be truncated by the secular approximation, due to the much larger shift differences among the spins.[63,64] As such, it is sufficient for us to consider only the $3S_{jz}S_{kz}$ terms for weak homonuclear dipolar interactions.

We consider the weak homonuclear coupling a bilinear interaction. When pulses are applied to a homonuclear spin pair, the RF acts on both spins, which is distinct from the cases of chemical shift and heteronuclear spin interactions where it acts on only one spin. Thus, the inversion of spin operators by an ideal refocusing pulse does not lead to the sign change of the density matrix influenced by the homonuclear spin Hamiltonian. It is well-known in solution-state NMR that homonuclear *J*-couplings modulate spin echoes, and their effects are not refocused by the Hahn-echo pulse sequence.[65,66] These concepts can be extended to the behavior of spins subjected to repeated refocusing pulses used in CPMG experiments; from this, we can understand how weak homonuclear dipolar couplings affect the T_2^{eff} and concomitant echo-train decay.

Herein, we explore how the weak homonuclear dipolar interaction manifests in CPMG echo trains and their corresponding spectra based on different refocusing pulse angles. Consideration is given to spin systems having a dominant linear (*i.e.*, CSA, SOQI) or traceless bilinear (*i.e.*, FOQI) interaction, along with weak homonuclear (*S*-*S*) dipolar coupling interactions. When refocusing pulses shorter than the standard $\theta = 180°$ (for dominant linear interactions) or $\theta = 90°$ (for traceless bilinear interactions) are used, respectively, the *S*-*S* dipolar dephasing is partially attenuated. This effect can be understood by consideration of the θ-REDOR pulse sequence and its application to heteronuclear (*S*-*I*) dipolar coupled systems, where

the refocusing of one of the heteronuclear spin pairs can be changed arbitrarily while others are kept at the ideal refocusing condition. Reducing the fraction of the spin states with heteronuclear coupled *I* spins with a $\theta < 180°$ pulse on the *I*-channel minimizes the number of *I* spins contributing to the dipolar dephasing of the *S* signal.[67] Smaller values of θ result in reduced contributions from the coupled *I* spins to dipolar dephasing/modulations that impact echo refocusing and formation. These effects are also exploited in SECSY, E-COSY, and bilinear-COSY pulse sequences that use small θ-refocusing pulses to minimize the evolution of spin polarization under bilinear *J*-coupling terms.[68–71] It may be possible to exploit this phenomenon to reduce the attenuation of the transverse spin polarization under weak homonuclear dipolar coupling in CPMG echo trains with small θ-refocusing pulses, while simultaneously refocusing transverse spin polarization evolving under the dominant anisotropic NMR interaction.

In the following sections, we describe the use of CPMG or CP-CPMG pulse sequences under static and MAS conditions with a fixed RF amplitude ν_1 for excitation and refocusing pulses (unless otherwise stated), where the excitation pulse width, τ_{exc}, is fixed (**Figure S1**). In experiments and simulations, the refocusing pulse width, τ_{ref}, is arrayed such that the refocusing flip angle, $\theta = 360\nu_1\tau_{ref}$ (in degrees), changes accordingly; the resulting FIDs, powder patterns, and integrated pattern areas are compared. Herein, it is shown that in the presence of weak homonuclear dipolar interactions, small flip angles resulting from short refocusing pulses reduce the dephasing effects of homonuclear dipolar interactions in CPMG echo trains, leading to increased values of T_2^{eff} and concomitant signal enhancement in comparison to conventional refocusing flip angles. It is observed that the signal enhancements and optimal θ values vary between individual samples based on their homonuclear dipolar constants, intrinsic T_2's, and

other factors. Experimental ^{13}C ($I = 1/2$), ^{2}H ($I = 1$), ^{87}Rb ($I = 3/2$), ^{23}Na ($I = 3/2$), and ^{35}Cl ($I = 3/2$) NMR and spin-density matrix simulations are discussed.

3.2 ^{13}C SSNMR Experiments

The static ^{1}H-^{13}C CP-CPMG NMR spectra (**Figure 1**) of isotopically enriched 1,2-phthalic anhydride-$^{13}C_2$ feature a wideline pattern that is primarily influenced by a large CSA, as well as significant contributions from homonuclear dipolar broadening due to the short ^{13}C-^{13}C bond (the dipolar coupling, $\nu_D \approx 2790$ Hz).[72] This sample is ideal for testing the effects of weak homonuclear dipolar coupling on CPMG echo trains, since it is isotopically enriched and approximates an isolated homonuclear spin pair; therefore, we anticipate the observation of significant effects from the dipolar coupling. The two ^{13}C-labeled sites are magnetically non-equivalent in the solid state, with δ_{33} oriented orthogonally to the ring plane, and δ_{22} tilted by an azimuthal angle of $\alpha = 24°$ from the C-C bond;[72] however, a better fit of the spectra acquired at a higher magnetic field is obtained in the current work using $\alpha = 35°$ (**Figure S2**). Initial CPMG experiments feature different flip angles for refocusing pulses, initially under static conditions, to see which values of θ lead to powder patterns having uniform appearance and maximal integrated area. After the CP contact period and echo delay time, a CPMG pulse sequence employing refocusing pulses with RF amplitudes of 100 kHz are used, where the refocusing pulse width, τ_{ref}, is varied from $\tau_{ref} = 5$ μs ($\theta = 180°$) to $\tau_{ref} = 1.25$ μs ($\theta = 45°$) (**Figure 1**). In each experiment, the time-domain CPMG echo train is recorded, from which the T_2^{eff} is measured, and subsequent echo coaddition and Fourier transform give the corresponding ^{13}C powder pattern. The pattern areas are measured by integration and compared to that of the $\tau_{ref} = 5$ μs ($\theta = 180°$) experiment, which is normalized to 1.00 (**Figure 1a**). Echo trains are fit with a

monoexponential decay function of the form $a \cdot \exp[-\tau/T_2^{eff}]$ to approximately measure the differences in effective coherence lifetimes between experiments; however, the echo trains will simultaneously encode oscillations originating from anisotropic dipolar couplings and these effects are not included in the fit for simplicity. For example, in the τ_{ref} = 5 μs (θ = 180°) experiment (**Figure 1a**), the echo train features echoes of varying intensity that oscillate between relatively low and high signal intensities. The corresponding powder pattern is distorted and does not resemble a typical ^{13}C CSA or dipolar pattern. As τ_{ref} decreases from 5 μs, corresponding to smaller flip angles, the powder pattern area increases, until a maximum is reached at τ_{ref} = 2.5 μs (90°); at this point, a 3.2-fold increase in area is observed, and the powder pattern resembles that in a conventional CSA and dipolar-broadened spectrum (**Figure 1d**). After this point, the area decreases for shorter pulse widths. The T_2^{eff} also increases with respect to that of τ_{ref} = 5 μs (θ = 180°) when using a shorter τ_{ref} and is maximized when using τ_{ref} = 1.25 μs (θ = 45°), whereas pattern area is maximized with τ_{ref} = 2.5 μs (θ = 90°).[56,57] It is difficult to accurately quantify T_2^{eff} in this case since the dipolar oscillations are not included in the fit, however these experiments may be useful in extracting information on the dipolar coupling.[67,73] Regardless of the τ_{ref} used, the second echo in the CPMG train is never fully formed, likely to residual dipolar oscillations; therefore, that echo is not included for T_2^{eff} fits. Small θ < 180° refocusing pulses encode less dipolar oscillations in the CPMG echo trains where the envelope of the train becomes more monoexponential with decreasing θ; however, the dipolar oscillations cannot be fully removed when using a small θ.[30]

180° refocusing pulses would be expected to optimally refocus isochromats evolving under the influence of the CSA in the absence of any other interactions. However, an increased T_2^{eff} and signal enhancement is obtained around τ_{ref} = 2.5 μs (90°) in comparison to the τ_{ref} = 5.0

μs (180°) experiment (**Figure 1**). As described above, values of θ that are < 180° will reduce the dipolar dephasing in cases where the *S*-*S* coupled spins evolve under a weak homonuclear dipolar coupling interaction, which for CPMG pulse sequences, leads to increased pattern areas and longer measured values of T_2^{eff}. These results suggest a balance needs to be struck between reducing the homonuclear dipolar dephasing via the use of small θ refocusing pulses (< 180°) that allow for the acquisition of more spin echoes, while also causing minimal losses from the sub-optimal refocusing of the spin polarization evolving under the influence of CSA. The optimal value of θ that is required to achieve this balance varies between spin systems, and can depend on the relative size of the homonuclear dipolar coupling constant(s), the number of coupled spins, relative CS and dipolar tensor orientations, and the intrinsic T_2 of the system.

The effects of homonuclear dipolar coupling are further explored using numerical simulations of experiments using a CPMG pulse sequence with maximum RF amplitude of 100 kHz, τ_{exc} = 2.5 μs (90°), and τ_{ref} varied between 5 μs and 0.5 μs. The AB spin system consists of the two magnetically non-equivalent ^{13}C spin CS tensors that only differ by the orientation of their δ_{11} and δ_{22} components (*vide supra* and **Figure S2**) and features an array of dipolar coupling constants, ν_D. The resulting contour plot shows a maximum powder pattern area, as indicated by the intensity (in arbitrary units), for ν_D = 0 Hz and τ_{ref} = 5.0 μs (180°) (**Figure 2a**), consistent with refocusing of isochromats in a CSA-dominated pattern. When $\nu_D \gtrsim 100$ Hz, maximum pattern area is observed for cases with τ_{ref} = 2.5 μs (90°), whereas cases with τ_{ref} = 5.0 μs (180°) are found to have lower relative areas. Examples of the FIDs and spectra are shown for the case of two overlapping CSA powder patterns with ν_D = 0 Hz (**Figure 2b**, **2c**). Maximum area (1.0) is observed for τ_{ref} = 5.0 μs (180°) pulses (**Figure 2b**), and a reduction by a factor of $1/\sqrt{2}$ is observed for τ_{ref} = 2.5 μs (90°) pulses (*i.e.*, the projection of spin polarization into the *xy*-

plane is scaled by cos(45°) = 0.71) (**Figure 2c**). When the homonuclear dipolar coupling of ν_D = 2790 Hz is used in the simulation, 180° refocusing pulses perform poorly, yielding a spectrum with a non-uniform pattern (**Figure 2d**). By comparison, 90° refocusing pulses yield a spectrum with a large signal enhancement relative to the 180° pulses and matches well with the experimental result (**Figure 2e**, *cf*. **Figure 1d**). It may be difficult to quantitatively replicate experimental conditions and results since intrinsic T_2's or T_2^{eff}'s cannot be included in numerical simulations in SIMPSON, and potential longer-range, intermolecular couplings are not considered.

MAS is widely used in SSNMR for averaging the manifestation of second-rank anisotropic spin interactions such as CSA, leading to high-resolution NMR spectra with isotropic chemical shifts in some cases. When the spinning rate (in Hz) is smaller or on the order of the anisotropy, spinning sideband (SSB) manifolds are observed with envelopes that somewhat resemble the static CSA powder patterns.[74,75] For strongly coupled spin systems, such as those with many homonuclear dipolar coupled protons, MAS only averages the effects of dipolar coupling to first order. Residual line widths under MAS from higher orders are highly sensitive to spinning speed.[76–78] For weakly coupled spins, the degree to which MAS averages the dipolar coupling is highly dependent on the isotropic shift difference between the two spins, which can cause R^2 recoupling (*vide supra*).

The two labeled sites of 1,2-phthalic anhydride-$^{13}C_2$ have the same isotropic chemical shift, meeting the requirement for the $n = 0$ R^2 condition, since they are rendered magnetically distinct from one another due to their distinct CS tensor orientations. High-resolution CP/MAS spectra are used to observe the R^2 recoupling, then CP-CPMG/MAS is used to test dipolar coupling effects on CPMG echo trains. The effects of homonuclear dipolar recoupling are clearly

noticeable in ^{1}H-^{13}C CP/MAS NMR spectra acquired at spinning frequencies of 3 and 5 kHz (**Figure 3a**, **3b**); we note that the $n = 0$ R^2 condition is always satisfied independent of the spinning speed, though the magnitude of the recoupled interaction depends on the spinning speed, as indicated by the splittings in the spinning sidebands (SSBs). The effects of recoupling become smaller than the SSB linewidth at $\nu_{rot} = 10$ kHz (**Figure 3c**). Substantial effects from the homonuclear dipolar coupling are also observed in ^{1}H-^{13}C CP-CPMG/MAS NMR spectra acquired at $\nu_{rot} = 5$ kHz (**Figure 4a**, **4b**) and 3 kHz (**Figure 4c**, **4d**). The dipolar splittings in the SSB's are present in these CPMG spectra, but less resolved in comparison to those in spectra acquired with conventional ^{1}H-^{13}C CP/MAS, due to both reduced resolution from windowed acquisition during CPMG that maximizes the number of echoes and the application of Gaussian line broadening that attenuates sinc artifacts.

At both spinning frequencies, significant signal enhancements resulting from reduced dipolar dephasing and concomitant increases in T_2^{eff} occur for experiments implementing $\tau_{ref} = 2.5$ μs (90°) in comparison to those employing $\tau_{ref} = 5.0$ μs (180°) (**Figure 4**). This enhancement is much smaller than the static case, though this is to be expected since the effective ν_D (*i.e.*, ν_D^{eff}) under MAS is reduced in comparison to the ν_D under static conditions. Significant oscillations in the echo trains are still evident at both spinning frequencies for $\tau_{ref} = 5$ μs (180°) (**Figure 4a**, **4c**) and are significantly attenuated with $\tau_{ref} = 2.5$ μs (90°) (**Figure 4b**, **4d**), just like the static case. On a side note, we did not observe analogous homonuclear dipolar coupling effects in our previous study featuring CPMG-MAS NMR experiments on spin-1/2 nuclei such as ^{119}Sn (n.a. = 8.6 %), ^{195}Pt (n.a. = 33.8 %), and ^{207}Pb (n.a. = 22.1 %); this is likely due to both a reduced number of homonuclear dipolar couplings and smaller ν_D^{eff} arising from the combination of lower natural abundances of these isotopes and increased nuclear distances.[58] In addition,

homonuclear coupling by the $n = 0$ R^2 condition requires differences in CSA modulated by MAS,[51] where CSAs vary among samples. Observations of augmented T_2^{eff}'s similar to those reported in the current work were reported by Cowans and Grutzner for rotor-synchronized ^{1}H-^{13}C CP-CPMG experiments in which different composite pulse widths for refocusing were compared;[79] however, the effects of homonuclear dipolar couplings were not discussed. More detailed analyses of dipolar effects in CPMG echo trains were described by Barret *et al.*, but consideration was not given to the effect of variable flip angles used in the CPMG pulse sequence.[80–82]

3.3 ^{2}H Experiments

Consideration is now given to the performance of (Q)CPMG pulse sequences on ^{2}H nuclei that experience weak homonuclear dipolar couplings and have powder patterns that are influenced by substantial FOQI broadening. It is well known that $\theta = 90°$ refocusing pulses in (Q)CPMG pulse sequences refocus the spin polarization influenced by the FOQI,[6–9] and when simultaneous paramagnetic or CSA interactions are present, a combination of interleaved $\theta = 180°$ and $\theta = 90°$ can refocus both interactions;[11,12,83,84] however, the impact of weak ^{2}H-^{2}H dipolar couplings has not been explored for CPMG sequences to date. Several samples featuring unique labeling schemes and concentrations, different sets of effective ^{2}H-^{2}H distances (r_D), and therefore, unique sets of homonuclear dipolar coupling constants, were studied using (Q)CPMG pulse sequences (**Table I**, see the supporting information for figures of all of the echo trains and spectra, **Figure S3 – S7**). In every case, a maximum RF amplitude of 100 kHz is used for excitation and refocusing, $\tau_{exc} = 2.5$ μs, and τ_{ref} is varied between 2.5 μs (90°) and 0.75 μs (27°).

For each case, we report T_2^{eff}'s and the ratio of the powder pattern areas from the CPMG experiments using conventional 90° and θ < 90° refocusing pulses (**Table I**).

Different flip angles for refocusing pulses were first tested in a (Q)CPMG pulse sequence for ^{2}H NMR of α-glycine-d_2 under static conditions (**Figure 5**). As τ_{ref} decreases from 2.5 μs, corresponding to smaller flip angles, the powder pattern area increases, until a maximum is reached at τ_{ref} = 1.25 μs (45°), for which a 1.9-fold increase in area is observed (**Figure 5f**). After this point, the area decreases with decreasing pulse widths. The T_2^{eff} also increases with progressively shorter refocusing pulse widths. However, its maximum value is not observed for the pattern of maximum area; rather, it continues to increase with decreasing pulse widths (**Figure S8)**. The first echo in each CPMG train progressively loses intensity for decreasing τ_{ref} with respect to the first echo formed in the experiment using τ_{ref} = 2.5 μs (θ = 90°) and the second and third echoes continue to lose intensity below τ_{ref} = 1.25 μs (the reasons for this are explored with numerical simulations, *vide infra*); as such, the first three echoes are not included in the T_2^{eff} fits for these reasons. It is important to note that the significant increases in pattern area with θ < 90° are not a consequence of increased refocusing-pulse bandwidths, as can be readily observed by examining isochromat intensities around the transmitter (*i.e.*, 0 Hz offset).

In α-glycine-d_2, there is a short distance between the -CD_2 deuterons of r_D = 1.817 Å, giving rise to a homonuclear dipolar coupling of ν_D = 472 Hz (**Table I**); to a good approximation, this system is regarded as having an isolated ^{2}H-^{2}H spin pair, though there may be multiple, smaller intermolecular dipolar couplings. Small θ-refocusing pulses can attenuate dipolar dephasing significantly in the CPMG echo trains of ^{2}H nuclei simultaneously influenced by the dominant bilinear FOQI and weak homonuclear dipolar couplings. These effects are

further studied using both simulations and additional experiments on distinct spin systems that include varying numbers of homonuclear dipolar couplings of different magnitudes.

Numerical simulations of a CPMG pulse sequence were conducted for the ^{2}H-^{2}H spin pair in α-glycine-d_2 using previously reported EFG tensor parameters.[85,86] The sequence uses a RF amplitude of 100 kHz and τ_{exc} = 2.5 μs with values of ν_D that vary between 0 and 1000 Hz and τ_{ref} that range from 2.5 μs to 0.75 μs. The resulting contour plot (**Figure 6a**) shows maximum pattern area at τ_{ref} = 2.5 μs (90°) for ν_D = 0 Hz, as would be expected for refocusing isochromats evolving solely under the FOQI. For $\nu_D \gtrsim 400$ Hz, local maxima are apparent at τ_{ref} = 1.5 μs (54°), whereas τ_{ref} = 2.5 μs (90°) yields less intensity by comparison, in relatively good agreement with experimentally observing maximum enhancement withτ_{ref} = 1.25 μs (45°). The simulated FID for ν_D = 0 Hz and τ_{ref} = 2.5 μs (90°) has an echo train with a relatively flat profile, since there is no T_2 decay included in SIMPSON simulations (**Figure 6b**). The simulated FID for ν_D = 0 Hz and τ_{ref} = 1.5 μs (54°) (**Figure 6c**) has an initial echo that is substantially less intense than the τ_{ref} = 2.5 μs (90°) case, which is a common observation for CPMG echo trains employing a small θ;[10,56] this effect can be further understood by considering initial zero-quantum coherence (ZQC) generation (*cf.* **Figure S9**). The experimental echo trains also show a loss of intensity in the first echo and increased T_2^{eff} as the refocusing pulse width is decreased, even below 1.5 and 1.25 μs (*cf.* **Figure 5e-h** and **Figure S8**). In simulations, the areas of the powder patterns for τ_{ref} = 1.5 μs (54°) are reduced with respect to that of τ_{ref} = 2.5 μs (90°) (*cf.* **Figure 6b, 6c**), which is consistent with 90° refocusing pulses as the best choice in quadrupolar-echo or QCPMG-type pulse sequences for optimal refocusing of isochromats evolving solely under the FOQI.[6,7,83]

Similar numerical calculations were carried out with ν_D = 450 kHz; FIDs and patterns for the τ_{ref} = 2.5 μs (90°) and τ_{ref} = 1.5 μs (54°) cases are shown in **Figure 6d** and **Figure 6e**, respectively. The magnitude of the echo train in the former case reveals an apparent oscillation that originates from the time-propagation of the homonuclear dipolar Hamiltonian. Interestingly, this oscillation effectively reduces the intensity of several spin echoes, especially those early in the echo train. In the latter case, this oscillation is attenuated, leading to higher overall signal in the echo train and powder pattern, as indicated by the normalized area (*cf.* **Figure 6d, 6e**). If refocusing pulses with θ < 90° are used in a CPMG experiment for spin-1 nuclei, the effects of the homonuclear dipolar coupling are reduced, leading to an increase in the measured value of T_2^{eff} and pattern area. Again, quantitative simulated results are difficult to achieve since intrinsic T_2's and potential intermolecular couplings are not considered, the latter of which may also affect the dipolar oscillations observed in simulations as compared to experiments.

We note that careful consideration must be given to the inter-echo delay, since this can also augment or reduce T_2^{eff} for homonuclear dipolar coupled systems.[80–82,87] The windowed acquisition period (i) depends on the inter-echo delay and (ii) must be large enough to capture the entire echo. Therefore, it is recommended to use a fixed inter-echo delay time and use variable refocusing pulse widths, rather than varying echo delays, to increase T_2^{eff}'s in homonuclear dipolar coupled systems.

Additional samples, including urea-d_4 and 1,8-dimethylnapthelene (DMNAP)-d_{12}, both demonstrate a significant increase in the $T_2^{eff,45}$ in comparison to $T_2^{eff,90}$ (*i.e.,* the values of T_2^{eff} measured with θ = 45° and 90°, respectively), as well as overall signal enhancements, likely owing to relatively strong homonuclear dipolar couplings in these systems (**Figures S3**, **S4**). In the case of DMNAP-d_{12}, the maximum enhancement is observed for a τ_{ref} = 1.0 μs (36°) pulse

(**Table I**). This difference may originate, in part, from its more complex homonuclear coupling behavior, since it is uniformly labeled and there are numerous intra- and intermolecular couplings between deuterons, as well as the differences in the intrinsic T_2's of these systems[88] Nonetheless, the shorter refocusing pulse clearly augments the T_2^{eff} and enhances signal with respect to conventional 90° refocusing pulses, consistent with our simulations on an isolated ^{2}H-^{2}H spin pair.

Several samples, including benzoic acid-*d*, MIL-53-d_4, and dimedone-*d*, have smaller and/or fewer couplings; experiments analogous to those above reveal either a small T_2^{eff} augmentation and/or signal enhancement, or a reduction of signal intensity (**Figures S5**, **S6**, and **S7**). The strongest coupling for benzoic acid-*d* is only slightly less than that of DMNAP-d_{12}, and yet, a reduction in signal intensity is observed when τ_{ref} = 1.25 μs (45°) is used. Unlike DMNAP-d_{12}, with its multiple homonuclear dipolar couplings, benzoic acid-*d*, which forms a dimer in the solid state, is only labelled at the carboxylic acid site, and primarily appears as an isolated spin pair (AB system); this means that there is only a single homonuclear coupling in the latter case.[89] Furthermore, ^{1}H decoupling with an RF field of 50 kHz is necessary for benzoic acid-*d*, which places restrictions on acquisition windows and decoupling fields (N.B.: ^{1}H decoupling can also augment T_2^{eff}). Decoupling for acquisition periods longer than *ca*. 50 ms is not advisable due to limitations on the duty cycle of our probe. The use of τ_{ref} = 1.25 μs (45°) extends the T_2^{eff} decay well beyond 50 ms, which may result in a net signal enhancement if those additional echoes are acquired; however, in the limited acquisition window, the shorter refocusing pulses yield a net decrease in signal. In addition, the H/D atoms of the carboxylic acid in the benzoic acid dimer undergo exchange, which may partially average the ^{2}H-^{2}H dipolar coupling, resulting in a weaker effective coupling strength.[89,90] The T_2^{eff} decay of MIL-53-d_4 is well within the sampling

window and a small 1.08-fold signal enhancement is observed, likely owing to the relatively smaller ν_D = 208 Hz (**Figure S6**).[49] MIL-53-d_4 is also used to demonstrate that creating 45° refocusing-pulse nutation by fixing the pulse width at 2.5 μs and decreasing the RF amplitude to 50 kHz, yields a very similar result to adjusting the pulse width and fixing the amplitude. Finally, dimedone-*d* features the weakest coupling (ν_D = *ca.* 22 Hz) and signal is reduced from the application of shorter refocusing pulses (**Figure S7**). The T_2^{eff} is somewhat enhanced with 45° refocusing pulses, but this is likely because of ZQC generation, as described in simulations (*vide supra*, **Figure S9**).

Final consideration is given to the previously reported signal enhancement for ^{2}H NMR of α-glycine-d_2 under MAS conditions with the use of 45° refocusing pulses for CPMG that was conducted by our research group.[58] Gan and Robyr previously described homonuclear dipolar recoupling *via* a $n = 0$ R^2 condition for this sample under MAS because the two -CD_2 deuterons are non-equivalent due to different EFG tensor parameters and orientations.[43] Our previously reported experiments featured maximum RF amplitudes of 75 kHz, an τ_{exc} = 3.33 μs, and various refocusing pulse widths, where τ_{ref} = 1.67 μs corresponds to a 45° refocusing pulse in this case. Reexamining this data shows that the T_2^{eff} under MAS is enhanced from 26.8 ms to 63.7 ms and the integrated area under the spinning side bands is enhanced by a factor of 1.17 (**Figure 7**). This enhancement factor is again smaller than that of the static case due to the reduced ν_D^{eff} under MAS. The same result is achieved using 45° refocusing pulses after a CP contact period in CP-CPMG/MAS.[58] It is anticipated that dipolar refocusing can be exploited for signal enhancement in other deuterated systems that experience homonuclear dipolar coupling under static and MAS conditions. This phenomenon may be potentially useful for distance measurements between deuterons.

3.4 Experiments on Half-Integer Quadrupolar Nuclei

We now consider the influence of weak homonuclear dipolar coupling in CPMG experiments on half-integer spin quadrupolar nuclei, which comprise 74 % of NMR-active isotopes. Three different $I = 3/2$ cases are investigated, involving a range of distinct homonuclear dipolar coupling scenarios, including: (i) ^{87}Rb (n.a. = 27.83%) of $RbNO_3$, with a moderate $\nu_D \approx$ 227 Hz; (ii) ^{23}Na (n.a. = 100%) of Na_2SO_4, with a moderate $\nu_D \approx 245$ Hz; and (iii) ^{35}Cl (n.a. = 75.78%) of L-histidine $HCl \cdot H_2O$, with a negligible $\nu_D \approx 6$ Hz. The values of ν_D listed above correspond to the shortest reported r_D, for simplification of comparing relative coupling strengths between compounds (**Table II**). We note that two of these systems, $RbNO_3$ and Na_2SO_4, also have extensive dipolar coupling networks, especially the latter (*vide infra*). For these nuclei, RF amplitudes of 10 kHz were used in CPMG pulse sequences with CT-selective pulse widths, where pulse widths of 25 μs and 12.5 μs cause CT-selective flip angles (θ_{sel}) of 180° and 90°, respectively. In this section, the flip angles are always considered as CT selective, a $\tau_{exc} = 12.5$ μs (90°) is used for excitation, and various refocusing flip angles are tested. Numerical simulations are also presented for a generic case of a dipolar-coupled spin pair of $I = 3/2$ nuclei. These tests are distinct from the work of Grandinetti *et al.*, where weak RF irradiation with fixed $\theta_{ref}^{sel} = 180°$ was used for substantial T_2^{eff} enhancements as the result of excitation and refocusing that is highly selective to the CT and avoids any coherence loss to the STs under MAS (*vide infra*).[17] Consideration is not given to the impact of residual dipolar coupling between quadrupolar nuclei under MAS in these cases.[40,91]

The first case is that of ^{87}Rb NMR of $RbNO_3$, which based on internuclear ^{87}Rb-^{87}Rb distances, is expected to have a maximum $\nu_D \approx 227$ Hz (**Table II**). Under static conditions, a

large T_2^{eff} enhancement and signal enhancement of 2.61 is observed in spectra acquired using $\theta_{ref}^{sel} = 90°$ in comparison to those acquired with $\theta_{ref}^{sel} = 180°$ (**Figure 8a**, **8b**). 90° refocusing pulses do not offer signal enhancement, likely due to spatiotemporal averaging of the dipolar interaction with $\nu_{rot} = 10$ kHz under MAS, resulting in signal loss of a *ca.* $1/\sqrt{2}$ (**Figure 8c**, **8d**). $RbNO_3$ has three sites with different shifts;[92–94] therefore, the $n = 0$ R^2 recoupling is much smaller among the non-equivalent sites, likely resulting in a negligible ν_D^{eff} at $\nu_{rot} = 10$ kHz. The corresponding T_2^{eff} is moderately enhanced (**Figure 8d**) but is likely due to zero-quantum coherence (ZQC) generation (*i.e.,* prolonged signal decay by refocusing stimulated and spin echoes, *vide infra*; *c.f.* **Figure S9**)[56,95] and does not yield signal enhancement. $RbNO_3$ is not known to experience an effective dipolar coupling between ^{87}Rb nuclei by R^2 recoupling alone at $\nu_{rot} = 10$ kHz.[94] In each case, the first two echoes are not included in the T_2^{eff} fits, since they are not fully formed in **Figure 8b**, **8d** with $\theta_{ref}^{sel} = 90°$ and result in a non-exponential decay; hence, only the remaining echoes are considered, since they appear to undergo an exponential decay. Multiple refocusing pulse widths were tested under static and MAS conditions, which show local minima of signal intensity when using the pulse sequence with $\tau_{ref} = 25$ μs (180°) when homonuclear dipolar coupling is present and small signal enhancements with different $\theta_{ref}^{sel} < 180°$ at $\nu_{rot} = 2$ and 5 kHz (**Figure S10**).

The second case is ^{23}Na NMR of Na_2SO_4, which was chosen due to the multiple couplings of ^{23}Na nuclei with close proximities (**Table II**), n.a. = 100 %, having five magnetically inequivalent sites, and previously reported evidence of the detection of effective dipolar coupling under MAS by $n = 0$ R^2 recoupling since there are no shifts amongst the sites.[44,96–98] Like the case of ^{87}Rb NMR, the static ^{23}Na CPMG experiment shows maximum signal enhancement with $\tau_{ref} < 25$ μs; however, unlike the ^{87}Rb case, this occurs for $\tau_{ref} = 10.0$ μs

(72°) with a 2.95-fold enhancement (**Figure 9a**, **9b** and **Figure S11**). Under MAS with ν_{rot} = 10 kHz, the T_2^{eff} is increased from 8.15 ms to 22.47 ms and a maximum signal enhancement of 2.44 is achieved with τ_{ref} = 12.5 μs (90°) (**Figure 9c**, **9d** and **Figure S11**). This is in contrast to the ^{87}Rb NMR case, as the homonuclear dipolar coupling between ^{23}Na nuclei is recoupled under MAS at ν_{rot} = 10 kHz for this sample.[44]

The final case is that of ^{35}Cl NMR of L-histidine HCl·H_2O, which features a single ^{35}Cl chemically distinct site and four magnetically inequivalent sites (assuming non-negligible dipolar couplings between ^{35}Cl nuclei),[99] was chosen with the anticipation that this homonuclear dipolar refocusing effect may not be observed for a ^{35}Cl spin pair, due to the much lower gyromagnetic ratio of ^{35}Cl (in comparison to those of ^{87}Rb and ^{23}Na) and their increased spatial separation (in this compound, $\nu_D \approx 6$ Hz; for this reason an MAS spectrum was not acquired) (**Table II**). Crucially, in a pulse width array under static conditions, a local minimum in signal intensity is observed with θ_{ref}^{sel} = 180° (**Figure S12**), similar to the characteristic signal depletions observed in static ^{87}Rb and ^{23}Na experiments (**Figures S10 and S11**). A longer T_2^{eff} and slight increase in the maximum pattern area are observed for τ_{ref} = 20 μs (144°) refocusing in this case (**Figure 10**). This result is surprising, as a depletion in signal intensity would be expected with θ_{ref}^{sel} < 180° for a spin pair solely influenced by the SOQI when the dipolar coupling constant is nearly negligible; hence, we investigated this further with numerical simulations.

The effects of homonuclear dipolar coupling on CPMG echo trains are examined for I = 3/2 nuclei with numerical simulations using a spin system comprised of two equivalent ^{23}Na spins with the same EFG tensor parameters as Na_2SO_4, with the largest component of their EFG tensors oriented at β = 90° with respect to the internuclear vector. Multiple orientations between the two EFG tensors and between the EFG and dipolar tensors were tested, which had little

impact on the simulated results. The impacts of different dipolar couplings and refocusing pulses (that vary from 50 to 2.5 μs, where τ_{ref} = 25 μs is a 180° refocusing pulse) on signal intensity are probed (**Figure 11a**). For ν_D = 0 Hz, a maximum pattern area is observed for τ_{ref} = 25 μs (180°); however, ν_D > 0 Hz and τ_{ref} = 25 μs (180°) results in local minima in pattern areas, even for small ν_D ~ 5 Hz. For $\nu_D \geq$ 50 Hz, maximum signal intensities are observed for τ_{ref} = 15 or 17.5 μs, depending on the magnitude of ν_D. Some examples of FIDs and spectra for ν_D = 0 Hz (**Figure 11b, c**) demonstrate that τ_{ref} = 25 μs (180°) refocusing pulses again perform best. When ν_D = 250 Hz, some dipolar splittings are observed in the static pattern that do not completely match the static experimental ^{23}Na powder pattern (**Figure 11d, e**); this is due to our simulations involving only two spins, whereas the multiple homonuclear dipolar couplings in Na_2SO_4 exert a distinct influence on the appearance of the experimental powder patterns (*cf.* **Figure 9a**, **b**).[97] τ_{ref} = 15 μs (108°) now offers a signal enhancement in comparison to τ_{ref} = 25 μs (180°), which generally supports the hypothesis that shorter refocusing pulses yield uniform patterns of maximum areas in ^{87}Rb and ^{23}Na static experiments and ^{23}Na MAS experiments where homonuclear dipolar recoupling manifests. Simulations predict maximum signal enhancement for τ_{ref} = 20 μs (144°) when ν_D = 5 Hz for this spin system, which may explain the current experimental ^{35}Cl observations and previous observations of SNR enhancement with $\theta_{ref}^{sel} < 180°$ in ^{35}Cl NMR of Cp_2ZrCl_2.[10] These results suggest the possibility of probing distance measurements for a wide array of quadrupolar nuclei, particularly for cases of isolated spin pairs.

It is important to note that the mechanism for signal enhancement observed for half-integer quadrupolar nuclei in this work is not a consequence of the refocusing pulses with low RF amplitudes, as described by Grandinetti *et al.*[17] In their work, increases in T_2^{eff} are observed in ^{17}O and ^{33}S CPMG/MAS spectra acquired with low-power (highly selective) refocusing pulses

that are applied with a fixed $\theta_{ref}^{sel} = 180°$; corresponding enhancements are the result of avoiding coherence exchange with the STs by being highly selective for the CT. In the current work, ν_1 is instead fixed and τ_{ref} and θ_{ref}^{sel} are varied, leading to increased pattern areas and T_2^{eff}'s, arising from reduced contributions of homonuclear dipolar dephasing. Furthermore, enhancements are observed under both MAS and static conditions, the latter of which minimize coherence exchanges between the CT and STs.

3.5 Practical Guidelines

The following guidelines are recommended for the practical implementation of CPMG for systems with SSNMR spectra that experience weak homonuclear dipolar coupling:

1. The CPMG pulse sequence should be initiated with a 90° excitation pulse and the flip angle of the refocusing pulse, θ, should be arrayed either by (i) varying the pulse width with a fixed amplitude or by (ii) varying the pulse amplitude with a fixed width until the powder pattern area is maximized; however, the former is a more robust approach since this maximizes refocusing bandwidth.[58] The optimal θ that maximizes SNR varies between samples and can depend on factors such as intrinsic T_2 differences between samples, MAS spinning speeds, the number of homonuclear dipolar couplings between nuclei and their strengths, relative EFG or CS and dipolar tensor orientations, and accurate MAS settings for half-integer spin quadrupolar nuclei. Therefore, θ will likely vary between systems even when identical nuclei are being probed, but the examples covered in this work reflect sensible starting points and ranges of conditions to test.

2. For experiments under MAS, rotor-synchronization should be maintained using previously outlined conditions,[58] and consideration should be given to the possibility of the occurrence of R^2 recoupling that can allow homonuclear dipolar coupling effects to manifest.

3. (a) For systems that are primarily influenced by linear interactions, including CSA, paramagnetic broadening, and/or SOQI and are simultaneously influenced by weak homonuclear dipolar couplings, the optimal $\theta < 180°$ (including the CT selective θ_{sel} when $\nu_Q > \nu_1$). (b) For analogous systems where the dominant interaction is instead traceless and bilinear (*i.e.,* the FOQI where off-resonance effects are neglected) the optimal $\theta < 90°$.

4. Careful consideration should be given to measured T_2^{eff} exponential decay constants in systems that experience weak dipolar coupling, and their significance should be interpreted with caution. The envelope of the echo train will simultaneously encode an exponential decay and oscillations from the dipolar coupling, the latter of which are anisotropic under static conditions. The choice of refocusing pulse flip angle and the echo delay time can affect the measured T_2^{eff} and how the dipolar oscillations manifest.

4. Conclusions

CPMG-type pulse sequences that use short refocusing pulses with small θ flip angles can yield substantial signal enhancements in SSNMR spectra of weakly homonuclear dipolar coupled nuclei under both static and MAS conditions. In most cases, this results from a reduction in dipolar dephasing and concomitant increases in T_2^{eff}'s in comparison to conventional approaches for acquiring SSNMR spectra of such systems. When weak homonuclear dipolar coupling exists, small θ pulses attenuate the dipolar dephasing while also partially refocusing the dominant anisotropic interaction (where θ varies for dominant linear or

bilinear interactions, *vide supra*). A balance needs to be struck between maximizing the measured T_2^{eff} by using a small θ to reduce dipolar dephasing, while also minimizing losses of sub-optimal small-θ refocusing of the dominant anisotropic interaction. This has been demonstrated with ^{13}C NMR, ^{2}H-labelled samples having ^{2}H-^{2}H dipolar coupling constants of varying numbers and magnitudes, several $I = 3/2$ nuclei that experience various homonuclear dipolar coupling conditions, and numerical simulations on isolated spin pairs. Depending on the coupling conditions signal is enhanced by a factor as large as 3.2. The manifestation of this effect is strongest under static conditions, but is attenuated under MAS conditions, since the secular manifestation of the dipolar tensor is largely averaged in the latter case. However, under certain circumstances, R^2 recoupling can occur and partially reintroduce the homonuclear dipolar coupling under MAS, potentially allowing for T_2^{eff} enhancement by shorter refocusing pulses if effective dipolar couplings are strong enough. It is anticipated this effect may occur for systems that have common isotopes such as ^{2}H, ^{13}C, ^{15}N, and ^{17}O, but the degree to which it manifests will be strongly dependent on the degree of isotopic enrichment. This effect should also be observed for high-γ and high n.a. nuclei such as ^{11}B, ^{19}F, ^{27}Al, ^{31}P, *etc*. in most cases. It may be possible to use measured T_2^{eff}'s from variable refocusing flip angles and the dipolar oscillations in CPMG echo trains to establish internuclear distances in some cases. We anticipate that such modified CPMG pulse sequences that suppress weak homonuclear dipolar coupling can be readily applied to a multitude of NMR-active nuclei from across the periodic table, providing unique insights into structure and bonding.

5. Supplementary Material

See supplementary material for additional simulations, experiments, and experimental details.

6. Acknowledgments

R.W.S. and A.R.A would like to thank the National Science Foundation Chemical Measurement and Imaging Program, with partial co-funding from the Solid State and Materials Chemistry Program (NSF-2003854), for supporting this work. The National High Magnetic Field Laboratory is supported by the National Science Foundation through NSF/DMR-1644779 and the State of Florida. Adrian Gonzalez-Nelson is thanked for synthesising MIL-53(Al)-d_4 and Austin Peach is thanked for synthesizing benzoic acid-*d* and dimedone-*d*.

7. Data Availability

All simulation input files, pulse programs, and NMR datasets are available from the authors upon request.

8. References

(1) Carr, H. Y.; Purcell, E. M. *Phys. Rev.* **1954**, *94*, 630–638.

(2) Meiboom, S.; Gill, D. *Rev. Sci. Instrum.* **1958**, *29*, 688–691.

(3) Shore, S. E.; Ansermet, J.; Slichter, C. P.; Sinfelt, J. H. *Phys. Rev. Lett.* **1987**, *58*, 953–956.

(4) Barrett, S. E.; Durand, D. J.; Pennington, C. H.; Slichter, C. P.; Friedmann, T. A.; Rice, J. P.; Ginsberg, D. M. *Phys. Rev. B* **1990**, *41*, 6283–6296.

(5) De Soto, S. M.; Slichter, C. P.; Kini, A. M.; Wang, H. H.; Geiser, U.; Williams, J. M. *Phys. Rev. B* **1995**, *52*, 10364–10368.

(6) Bloom, M.; Sternin, E. *Biochemistry* **1987**, *26*, 2101–2105.

(7) Larsen, F. H.; Jakobsen, H. J.; Ellis, P. D.; Nielsen, N. C. *Chem. Phys. Lett.* **1998**, *292*, 467–473.

(8) Larsen, F. H. *Solid State Nucl. Magn. Reson.* **2007**, *31*, 100–114.

(9) Larsen, F. H. *Simulation of Molecular Motion of Quadrupolar Nuclei in Solid-State NMR Spectra*. In *Annual Reports on NMR Spectroscopy*; Elsevier Ltd, 2010; Vol. 71, pp 103–137.

(10) Hung, I.; Gan, Z. *J. Magn. Reson.* **2010**, *204*, 256–265.

(11) Iijima, T.; Nishimura, K. *Chem. Phys. Lett.* **2011**, *514*, 181–186.

(12) Iijima, T.; Shimizu, T.; Nishimura, K. *J. Magn. Reson.* **2015**, *251*, 57–64.

(13) O'Dell, L. A.; Schurko, R. W. *Chem. Phys. Lett.* **2008**, *464*, 97–102.

(14) Schurko, R. W. *Acquisition of Wideline Solid-State NMR Spectra of Quadrupolar Nuclei*. In *Encyclopedia of Magnetic Resonance*; John Wiley & Sons, Ltd: Chichester, UK, 2011; pp 77–93.

(15) Schurko, R. W. *Acc. Chem. Res.* **2013**, *46*, 1985–1995.

(16) O'Dell, L. A.; Rossini, A. J.; Schurko, R. W. *Chem. Phys. Lett.* **2009**, *468*, 330–335.

(17) Jardón-Álvarez, D.; Bovee, M. O.; Baltisberger, J. H.; Grandinetti, P. J. *Phys. Rev. B* **2019**, *100*, 140103.

(18) Jardón-álvarez, D.; Bovee, M. O.; Grandinetti, P. J. *J. Magn. Reson.* **2021**, 107097.

(19) Bennett, A. E.; Rienstra, C. M.; Auger, M.; Lakshmi, K. V.; Griffin, R. G. *J. Chem. Phys.* **1995**, *103*, 6951–6958.

(20) Hodgkinson, P. *Prog. Nucl. Magn. Reson. Spectrosc.* **2005**, *46*, 197–222.

(21) Siegel, R.; Nakashima, T. T.; Wasylishen, R. E. *J. Phys. Chem. B* **2004**, *108*, 2218–2226.

(22) Veinberg, S. L.; Friedl, Z. W.; Harris, K. J.; O'Dell, L. A.; Schurko, R. W. *CrystEngComm* **2015**, *17*, 5225–5236.

(23) Veinberg, S. L.; Friedl, Z. W.; Lindquist, A. W.; Kispal, B.; Harris, K. J.; O'Dell, L. A.; Schurko, R. W. *ChemPhysChem* **2016**, *17*, 4011–4027.

(24) Waugh, J. S.; Huber, L. M.; Haeberlen, U. *Phys. Rev. Lett.* **1968**, *20*, 180–182.

(25) Goldburg, W. I.; Lee, M. *Phys. Rev. Lett.* **1963**, *11*, 255–258.

(26) Sakellariou, D.; Lesage, A.; Hodgkinson, P.; Emsley, L. *Chem. Phys. Lett.* **2000**, *319*, 253–260.

(27) Paruzzo, F. M.; Emsley, L. *J. Magn. Reson.* **2019**, *309*, 106598.

(28) Ostroff, E. D.; Waugh, J. S. *Phys. Rev. Lett.* **1966**, *16*, 1097–1098.

(29) Mansfield, P.; Ware, D. *Phys. Lett.* **1966**, *22*, 133–135.

(30) Waugh, J. S.; Wang, C. H.; Huber, L. M.; Vold, R. L. *J. Chem. Phys.* **1968**, *48*, 662–670.

(31) Waugh, J. S.; Wang, C. H. *Phys. Rev.* **1967**, *162*, 209–216.

(32) Rhim, W.-K.; Burum, D. P.; Elleman, D. D. *Phys. Rev. Lett.* **1976**, *37*, 1764–1766.

(33) Vega, A. J.; Vaughan, R. W. *J. Chem. Phys.* **1978**, *68*, 1958–1966.

(34) Suwelack, D.; Waugh, J. S. *Phys. Rev. B* **1980**, *22*, 5110–5114.

(35) Siegel, R.; Nakashima, T. T.; Wasylishen, R. E. *Concepts Magn. Reson. Part A* **2005**, *26A*, 62–77.

(36) Andrew, E. R.; Bradbury, A.; Eades, R. G.; Wynn, V. T. *Phys. Lett.* **1963**, *4*, 99–100.

(37) Kubo, A.; McDowell, C. A. *J. Chem. Soc. Faraday Trans. 1 Phys. Chem. Condens. Phases* **1988**, *84*, 3713.

(38) Colombo, M. G.; Meier, B. H.; Ernst, R. R. *Chem. Phys. Lett.* **1988**, *146*, 189–196.

(39) Smith, S. O. *Encycl. Magn. Reson.* **2007**, 4–8.

(40) Edén, M. *Solid State Nucl. Magn. Reson.* **2009**, *36*, 1–10.

(41) Raleigh, D. P.; Levitt, M. H.; Griffin, R. G. *Chem. Phys. Lett.* **1988**, *146*, 71–76.

(42) Gan, Z.-H.; Grant, D. M. *Mol. Phys.* **1989**, *67*, 1419–1430.

(43) Gan, Z.; Robyr, P. *Mol. Phys.* **1998**, *95*, 1143–1152.

(44) Kwak, H.-T.; Srinivasan, P.; Quine, J.; Massiot, D.; Gan, Z. *Chem. Phys. Lett.* **2003**, *376*, 75–82.

(45) Iuga, D.; Morais, C.; Gan, Z.; Neuville, D. R.; Cormier, L.; Massiot, D. *J. Am. Chem. Soc.* **2005**, *127*, 11540–11541.

(46) Edén, M.; Frydman, L. *J. Phys. Chem. B* **2003**, *107*, 14598–14611.

(47) Khudozhitkov, A. E.; Jobic, H.; Freude, D.; Haase, J.; Kolokolov, D. I.; Stepanov, A. G. *J. Phys. Chem. C* **2016**, *120*, 21704–21709.

(48) Altenhof, A. R.; Lindquist, A. W.; Foster, L. D. D.; Holmes, S. T.; Schurko, R. W. *J. Magn. Reson.* **2019**, *309*, 106612.

(49) Gonzalez-Nelson, A.; Mula, S.; Šimėnas, M.; Balčiūnas, S.; Altenhof, A. R.; Vojvodin, C. S.; Canossa, S.; Banys, J.; Schurko, R. W.; Coudert, F.-X.; et al. *J. Am. Chem. Soc.* **2021**, *143*, 12053–12062.

(50) Gan, Z.-H.; Grant, D. M. *Chem. Phys. Lett.* **1990**, *168*, 304–308.

(51) Gan, Z.; Grant, D. M.; Ernst, R. R. *Chem. Phys. Lett.* **1996**, *254*, 349–357.

(52) Bak, M.; Rasmussen, J. T.; Nielsen, N. C. *J. Magn. Reson.* **2011**, *213*, 366–400.

(53) Edén, M. *Concepts Magn. Reson. Part A Bridg. Educ. Res.* **2003**, *18*, 24–55.

(54) Fenzke, D.; Freude, D.; Fröhlich, T.; Haase, J. *Chem. Phys. Lett.* **1984**, *111*, 171–175.

(55) Kentgens, A. P. M. *Geoderma* **1997**, *80*, 271–306.

(56) Hürlimann, M. .; Griffin, D. . *J. Magn. Reson.* **2000**, *143*, 120–135.

(57) Hürlimann, M. D. *J. Magn. Reson.* **2007**, *184*, 114–129.

(58) Altenhof, A. R.; Jaroszewicz, M. J.; Lindquist, A. W.; Foster, L. D. D.; Veinberg, S. L.; Schurko, R. W. *J. Phys. Chem. C* **2020**, *124*, 14730–14744.

(59) Mansfield, P. *Phys. Rev.* **1965**, *137*, A961–A974.

(60) Haeberlen, U.; Waugh, J. S. *Phys. Rev.* **1968**, *175*, 453–467.

(61) Schmidt-Rohr, K.; Saalwächter, K.; Liu, S.-F.; Hong, M. *J. Am. Chem. Soc.* **2001**, *123*, 7168–7169.

(62) Chen, H. Y.; Tycko, R. *J. Magn. Reson.* **2020**, *313*, 106715.

(63) Mehring, M. *Principles of High Resolution NMR in Solids*; Springer Berlin Heidelberg: Berlin, Heidelberg, 1983.

(64) Levitt, M. H. *Spin Dynamics*; John Wiley & Sons Ltd, 2008.

(65) Aue, W. P.; Karhan, J.; Ernst, R. R. *J. Chem. Phys.* **1976**, *64*, 4226–4227.

(66) Segawa, T. F.; Bodenhausen, G. *eMagRes* **2013**, *2*, 245–251.

(67) Gullion, T.; Pennington, C. H. *Chem. Phys. Lett.* **1998**, *290*, 88–93.

(68) Nagayama, K.; Wüthrich, K.; Ernst, R. R. *Biochem. Biophys. Res. Commun.* **1979**, *90*, 305–311.

(69) Griesinger, C.; Sørensen, O. W.; Ernst, R. R. *J. Am. Chem. Soc.* **1985**, *107*, 6394–6396.

(70) Griesinger, C.; Sørensen, O. .; Ernst, R. . *J. Magn. Reson.* **1987**, *75*, 474–492.

(71) Schulte-Herbrüggen, T.; Mádi, Z. L.; Sørensen, O. W.; Ernst, R. R. *Mol. Phys.* **1991**, *72*, 847–871.

(72) Orendt, A. M.; Facelli, J. C.; Radziszewski, J. G.; Horton, W. J.; Grant, D. M.; Michl, J. *J. Am. Chem. Soc.* **1996**, *118*, 846–852.

(73) Xue, X. *Solid State Nucl. Magn. Reson.* **2010**, *38*, 62–73.

(74) Maricq, M.; Waugh, J. S. *Chem. Phys. Lett.* **1977**, *47*, 327–329.

(75) Herzfeld, J.; Berger, A. E. *J. Chem. Phys.* **1980**, *73*, 6021–6030.

(76) Samoson, A.; Tuherm, T.; Gan, Z. *Solid State Nucl. Magn. Reson.* **2001**, *20*, 130–136.

(77) Chávez, M.; Wiegand, T.; Malär, A. A.; Meier, B. H.; Ernst, M. *Magn. Reson.* **2021**, *2*, 499–509.

(78) Simões de Almeida, B.; Moutzouri, P.; Stevanato, G.; Emsley, L. *J. Chem. Phys.* **2021**, *155*, 084201.

(79) Cowans, B. A.; Grutzner, J. B. *J. Magn. Reson. Ser. A* **1993**, *105*, 10–18.

(80) Dementyev, A. E.; Li, D.; MacLean, K.; Barrett, S. E. *Phys. Rev. B* **2003**, *68*, 153302.

(81) Li, D.; Dementyev, A. E.; Dong, Y.; Ramos, R. G.; Barrett, S. E. *Phys. Rev. Lett.* **2007**, *98*, 190401.

(82) Li, D.; Dong, Y.; Ramos, R. G.; Murray, J. D.; MacLean, K.; Dementyev, A. E.; Barrett, S. E. *Phys. Rev. B - Condens. Matter Mater. Phys.* **2008**, *77*, 1–26.

(83) Antonijevic, S.; Wimperis, S. *J. Magn. Reson.* **2003**, *164*, 343–350.

(84) Iijima, T.; Shimizu, T. *Solid State Nucl. Magn. Reson.* **2018**, *91*, 1–8.

(85) Müller, C.; Schajor, W.; Zimmermann, H.; Haeberlen, U. *J. Magn. Reson.* **1984**, *56*, 235–246.

(86) Aliev, A. E.; Mann, S. E.; Rahman, A. S.; McMillan, P. F.; Corà, F.; Iuga, D.; Hughes, C. E.; Harris, K. D. M. M.; Cora, F.; Iuga, D.; et al. *J. Phys. Chem. A* **2011**, *115*, 12201–12211.

(87) Ziener, C. H.; Kampf, T.; Jakob, P. M.; Bauer, W. R. *J. Magn. Reson.* **2010**, *202*, 38–42.

(88) Gan, Z.; Robyr, P.; Ernst, R. R. *Chem. Phys. Lett.* **1998**, *283*, 262–268.

(89) Stöckli, A.; Meier, B. H.; Kreis, R.; Meyer, R.; Ernst, R. R. *J. Chem. Phys.* **1990**, *93*, 1502–1520.

(90) Wu, G.; Hung, I.; Gan, Z.; Terskikh, V.; Kong, X. *J. Phys. Chem. A* **2019**, *123*, 8243–8253.

(91) Wi, S.; Frydman, L. *J. Chem. Phys.* **2000**, *112*, 3248–3261.

(92) Shamsuzzoha, M.; Lucas, B. W. *Acta Crystallogr. Sect. B Struct. Crystallogr. Cryst. Chem.* **1982**, *38*, 2353–2357.

(93) Massiot, D.; Touzo, B.; Trumeau, D.; Coutures, J. P.; Virlet, J.; Florian, P.; Grandinetti, P. J. *Solid State Nucl. Magn. Reson.* **1996**, *6*, 73–83.

(94) Iuga, D.; Holland, D.; Dupree, R. *J. Magn. Reson.* **2014**, *246*, 122–129.

(95) Wolf, T.; Jaroszewicz, M. J.; Frydman, L. *J. Phys. Chem. C* **2020**.

(96) Gee, B.; Eckert, H. *Solid State Nucl. Magn. Reson.* **1995**, *5*, 113–122.

(97) Duer, M. J. *Chem. Phys. Lett.* **1997**, *277*, 167–174.

(98) Duer, M. J.; Painter, A. J. *Chem. Phys. Lett.* **1999**, *313*, 763–770.

(99) Fuess, H.; Hohlwein, D.; Mason, S. A. *Acta Crystallogr. Sect. B Struct. Crystallogr.*

Cryst. Chem. **1977**, *33*, 654–659.

(100) Schreyer, M.; Guo, L.; Thirunahari, S.; Gao, F.; Garland, M. *J. Appl. Crystallogr.* **2014**, *47*, 659–667.

(101) Zavodnik, V.; Stash, A.; Tsirelson, V.; de Vries, R.; Feil, D. *Acta Crystallogr. Sect. B Struct. Sci.* **1999**, *55*, 45–54.

(102) Wilson, C. C.; Nowell, H. *New J. Chem.* **2000**, *24*, 1063–1066.

(103) Wilson, C. C.; Shankland, N.; Florence, A. J. *J. Chem. Soc. Faraday Trans.* **1996**, *92*, 5051.

(104) Ortiz, G.; Chaplais, G.; Paillaud, J.-L.; Nouali, H.; Patarin, J.; Raya, J.; Marichal, C. *J. Phys. Chem. C* **2014**, *118*, 22021–22029.

(105) Bolte, M.; Scholtyssik, M. *Acta Crystallogr. Sect. C Cryst. Struct. Commun.* **1997**, *53*, IUC9700013.

(106) Tanaka, K.; Naruse, H.; Morikawa, H.; Marumo, F. *Acta Crystallogr. Sect. B Struct. Sci.* **1991**, *47*, 581–588.

Tables

Table I: Homonuclear dipolar coupling constants, measured T_2^{eff}'s, and signal enhancements for ^{2}H-labelled samples in this work.

Sample	Shortest r_D (Å)[†]	ν_D (Hz)	$T_2^{eff,90}$ (ms)	$T_2^{eff,45}$ (ms)	S_{45}/S_{90}[‡]	Reference
α-glycine-d_2	1.817	472	3.19	11.96	1.90	[100]
Urea-d_4	1.739	538	1.09	3.33	1.33	[101]
DMNAP-d_{12}	2.124	295	2.64	8.36, 12.13[*]	1.49, 1.69[*]	[102]
Benzoic acid-d	2.262	245	48.8	74.22	0.81	[103]
MIL-53-d_4	2.387	208	8.224	23.11	1.08	[104]
Dimedone-d	5.030	22.2	22.14	31.33	0.84	[105]

[†] For samples that have multiple homonuclear dipolar couplings, the spin pair with the shortest average internuclear distance is reported, along with the corresponding dipolar coupling constant, ν_D.

[‡] The ratio of the integrated signal intensity of the powder patterns acquired with 45° and 90° refocusing pulses.

[*] Results using τ_{ref} = 1.0 μs (36°), which yielded the largest enhancements only in the case of DMNAP-d_{12}.

Table II: Homonuclear dipolar coupling constants of half-integer spin quadrupolar nuclei in samples in this work, measured T_2^{eff}'s, and signal enhancements.

Sample (Nucleus)	Shortest r_D (Å)†	ν_D (Hz)	ν_{rot} (kHz)	$T_2^{eff,180}$ (ms)	$T_2^{eff,\theta}$ (ms)*	S_θ/S_{90}‡	θ	Reference
$RbNO_3$ (^{87}Rb)	3.85	227	0	2.6	12.9	2.61	90	[92]
			10	62.6	82.6	0.77	90	
Na_2SO_4 (^{23}Na)	3.25	245	0	0.60	1.63	2.95	72	[106]
			10	8.15	22.47	2.44	90	
L-Histidine $HCl \cdot H_2O$ (^{35}Cl)	5.775	6	0	31.7	41.5	1.03	144	[99]

† For samples that have multiple homonuclear dipolar couplings, the spin pair with the shortest average internuclear distance is reported, along with the corresponding dipolar coupling constant, ν_D.

* The T_2^{eff} is measured when using a refocusing pulse of flip angle θ that varies between systems and experiments and is detailed in the text and the corresponding figures.

‡ The ratio of the integrated signal intensity of the powder pattern acquired with θ and 90° refocusing pulses.

Figure Captions

Figure 1. Experimental ^{1}H-^{13}C CP-CPMG NMR FIDs (left column) and spectra (right column) of 1,2-phthalic anhydride-$^{13}C_2$ acquired under static conditions using a RF amplitude of 100 kHz for all pulses, an excitation pulse width (τ_{exc}) of 2.5 μs, and a refocusing pulse width (τ_{ref}) that is varied between 5 μs – 1.25 μs (a – e) causing the refocusing pulse flip angle (θ) to change accordingly. In every case the area of the powder pattern is displayed to the right of the pattern and is normalized with respect to the pattern in (a). The FIDs and spectra in the left and right columns, respectively, are plotted on the same relative intensity scale. The monoexponential T_2^{eff}'s are denoted for each FID. In every case the second echo is not fully formed (see text for details); therefore, the second echo is not included for the T_2^{eff} fits.

Figure 2. Simulated ^{13}C NMR (a) powder pattern areas as a function of homonuclear dipolar couplings, ν_D, and refocusing pulse widths, τ_{ref}, with select FID's (middle column) and spectra (right column) of an AB spin system using CS tensor parameters of δ_{iso} = 131.67 ppm, Ω = 189.87 ppm, and κ = 0.37 for both sites, where the relative orientations of the two CS tensors is described in the main text (azimuthal angle, α = 35 °). Powder patterns are simulated with a CPMG pulse sequence using a RF amplitude of 100 kHz for all pulses, τ_{exc} = 2.5 μs, and a τ_{ref} that is varied (a) between 5 μs (180°) and 0.5 μs (18°). Select FIDs and spectra are shown for a τ_{ref} of (b) 5 μs (180°) and (c) 2.5 μs (90°) without a homonuclear dipolar coupling and (d, e) the same refocusing pulses, respectively, with ν_D = 2790 Hz. Blue lines show which set of FIDs and spectra correspond to which dipolar coupling strength in the contour plot. The areas are displayed to the right of each pattern and are normalized with respect to the pattern calculated with τ_{ref} = 5 μs (180°) in each case.

Figure 3. Experimental ^{1}H-^{13}C CP/MAS NMR FIDs and spectra of 1,2-phthalic anhydride-$^{13}C_2$ acquired with spinning frequencies of (a) 10 kHz, (b) 5 kHz, and (c) 3 kHz at 18.8 T.

Figure 4. Experimental ^{1}H-^{13}C CP-CPMG/MAS NMR FIDs (left column) and spectra (right column) of 1,2-phthalic anhydride-$^{13}C_2$ acquired with rotor frequencies of (a, b) 5 kHz and (c, d) 3 kHz. Signal is acquired using rotor-synchronized CP-CPMG/MAS with refocusing pulse amplitudes of 100 kHz and τ_{ref} of (a, c) 5 μs (180°) and (b, d) 2.5 μs (90°). The integrated areas of the spinning sideband manifolds are displayed to the right of the patterns and normalized with respect to the area pattern acquired with τ_{ref} = 5 μs (180°). The FIDs and spectra in the left and right columns, respectively, are plotted on the same intensity scale for purposes of separately comparing (a, b) 5 kHz MAS and (c, d) 3 kHz MAS data. The monoexponential T_2^{eff}'s are denoted for each FID.

Figure 5. Experimental ^{2}H NMR FIDs (left column) and spectra (right column) of α-glycine-d_2 acquired with a CPMG pulse sequence using a RF amplitude of 100 kHz for all pulses, an excitation pulse width (τ_{exc}) of 2.5 μs, and a refocusing pulse width (τ_{ref}) that is varied between 2.5 μs – 0.75 μs (a – h) causing the refocusing pulse flip angle (θ) to change accordingly. In every case the area of the powder pattern is displayed to the right of the pattern and is normalized with respect to the pattern in (a). The FIDs and spectra in the left and right columns, respectively, are plotted on the same relative intensity scale. The monoexponential T_2^{eff}'s are denoted for each FID. In every case the first three echoes are not included in the T_2^{eff} fits (see text for details).

Figure 6. (a) Areas of numerically simulated ^{2}H NMR powder patterns of an AB spin system as a function of homonuclear dipolar coupling strength and refocusing pulse widths and (b) - (e) select FIDs (middle column) and spectra (right column). The AB spin system has EFG tensor parameters of C_Q = 159.6 kHz and 167.6 kHz and η_Q = 0.058 and 0.084. With respect to a fixed EFG tensor for one site, the second EFG tensor is oriented at β = 109.5° and the dipolar tensor is oriented with β = 35.25°. Powder patterns are simulated with a CPMG pulse sequence using a RF amplitude of 100 kHz for all pulses, τ_{exc} = 2.5 μs, and a τ_{ref} that is varied (a) between 2.5 μs (90°) and 0.75 μs (27°). Select FIDs and spectra are shown for a τ_{ref} of (b) 2.5 μs (90°) and (c) 1.5 μs (54°) without a homonuclear dipolar coupling and (d, e) with ν_D = 450 Hz. Blue lines show which set of FIDs and spectra correspond to which dipolar coupling strength in the contour plot. The area of the powder pattern is displayed to the right and is normalized with respect to the pattern calculated with τ_{ref} = 2.5 μs (90°) in each case.

Figure 7. Experimental ^{2}H NMR FIDs (left column) and spectra (right column) of α-glycine-d_2 acquired under MAS with ν_{rot} = 10 kHz using a rotor-synchronized CPMG pulse sequence with RF amplitudes of 75 kHz for all pulses, τ_{exc} = 3.33 μs, and a τ_{ref} that is varied between (a) 3.33 μs (90°) and (b) 1.67 μs (45°). The areas of the spinning sideband manifolds are displayed to the right of each pattern, and are normalized with respect to the area of the pattern in (a). The FIDs and spectra in the left and right columns, respectively, are plotted on the same relative intensity scale. The monoexponential T_2^{eff}'s are denoted for each FID.

Figure 8. Experimental ^{87}Rb NMR FIDs (left column) and spectra (right column) of $RbNO_3$ acquired with a CPMG pulse sequence using a RF amplitude of 10 kHz for all pulses, τ_{exc} = 12.5 μs, and a τ_{ref} of (a) 25 μs (θ_{sel} = 180°) and (b) 12.5 μs (90°) under static conditions and (c, d) the same refocusing pulses, respectively, under MAS conditions with ν_{rot} = 10 kHz. The area of each powder pattern is displayed to its right, and is normalized with respect to the area of the pattern acquired with τ_{ref} = 25 μs (180°) in each case. The FIDs and spectra in the left and right columns, respectively, are plotted on the same intensity scale for purposes of separately comparing (a, b) static and (c, d) MAS data. The monoexponential T_2^{eff}'s are denoted for each FID. In every case the first two echoes are not included in the T_2^{eff} fits (see text for details).

Figure 9. Experimental ^{23}Na NMR FIDs (left column) and spectra (right column) of Na_2SO_4 acquired with a CPMG pulse sequence using a RF amplitude of 10 kHz for all pulses, τ_{exc} = 12.5 μs, and a τ_{ref} of (a) 25 μs (θ_{sel} = 180°) and (b) 12.5 μs (90°) under static conditions and (c, d) the same refocusing pulses, respectively, under MAS conditions with ν_{rot} = 10 kHz. The area of each powder pattern is displayed to its right, and is normalized with respect to the area of the pattern acquired with τ_{ref} = 25 μs (180°) in each case. The FIDs and spectra in the left and right columns, respectively, are plotted on the same intensity scale for purposes of separately comparing (a, b) static and (c, d) MAS data. The monoexponential T_2^{eff}'s are denoted for each FID.

Figure 10. Experimental ^{35}Cl NMR FIDs (left column) and spectra (right column) of L-histidine $HCl{\cdot}H_2O$ acquired under static conditions with a CPMG pulse sequence using a RF amplitude of 10 kHz for all pulses, τ_{exc} = 12.5 μs, and τ_{ref} that is varied between (a) 25 μs (θ_{sel} = 180°) and (b) 20 μs (144°). In each case the integral of the powder pattern is displayed to the right of the pattern and is normalized with respect to the pattern acquired with τ_{ref} = 25 μs (180°). The FIDs and spectra in the left and right columns, respectively, are plotted on the same intensity scale. The monoexponential T_2^{eff}'s are denoted for each FID.

Figure 11. Simulated ^{23}Na NMR (a) powder pattern areas as a function of homonuclear dipolar coupling strength and refocusing pulse widths and select FID's (middle column) and spectra (right column) of an A_2 spin system using EFG tensor parameters of C_Q = 2.6 MHz and η_Q = 0.6 for both sites. The largest component of both EFG tensors are oriented at β = 90° with respect to the internuclear vector. Powder patterns are simulated with a CPMG pulse sequence using a RF amplitude of 10 kHz for all pulses, τ_{exc} = 12.5 μs, and τ_{ref} that is varied (a) between 50 μs (θ_{sel} = 360°) and 2.5 μs (18°). Select FIDs and spectra are shown for a τ_{ref} of (b) 25 μs (180°) and (c) 15 μs (108°) ν_D = 0 Hz and (d, e) with ν_D = 250 Hz. Blue lines show which set of FIDs and spectra correspond to which dipolar coupling strength in the contour plot. The integral of the powder pattern is displayed to the right of each pattern and is normalized with respect to the pattern calculated with τ_{ref} = 25 μs (180°) in each case.

Figure 1

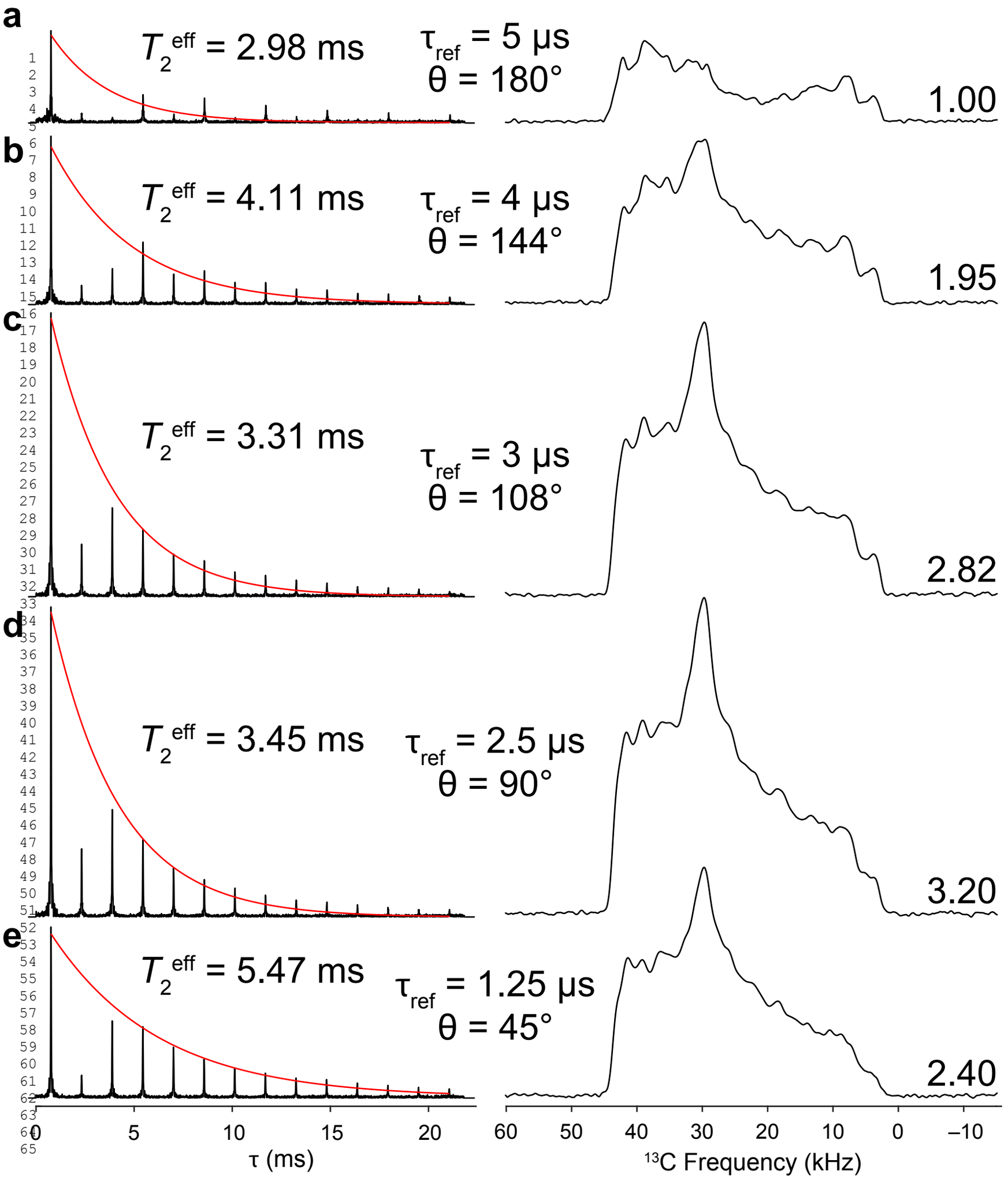
a
T_2^{eff} = 2.98 ms
τ_{ref} = 5 µs
θ = 180°
1.00
b
T_2^{eff} = 4.11 ms
τ_{ref} = 4 µs
θ = 144°
1.95
c
T_2^{eff} = 3.31 ms
τ_{ref} = 3 µs
θ = 108°
2.82
d
T_2^{eff} = 3.45 ms
τ_{ref} = 2.5 µs
θ = 90°
3.20
e
T_2^{eff} = 5.47 ms
τ_{ref} = 1.25 µs
θ = 45°
2.40
0
5
10
15
20
τ (ms)
60
50
40
30
20
10
0
–10
^{13}C Frequency (kHz)

Figure 2

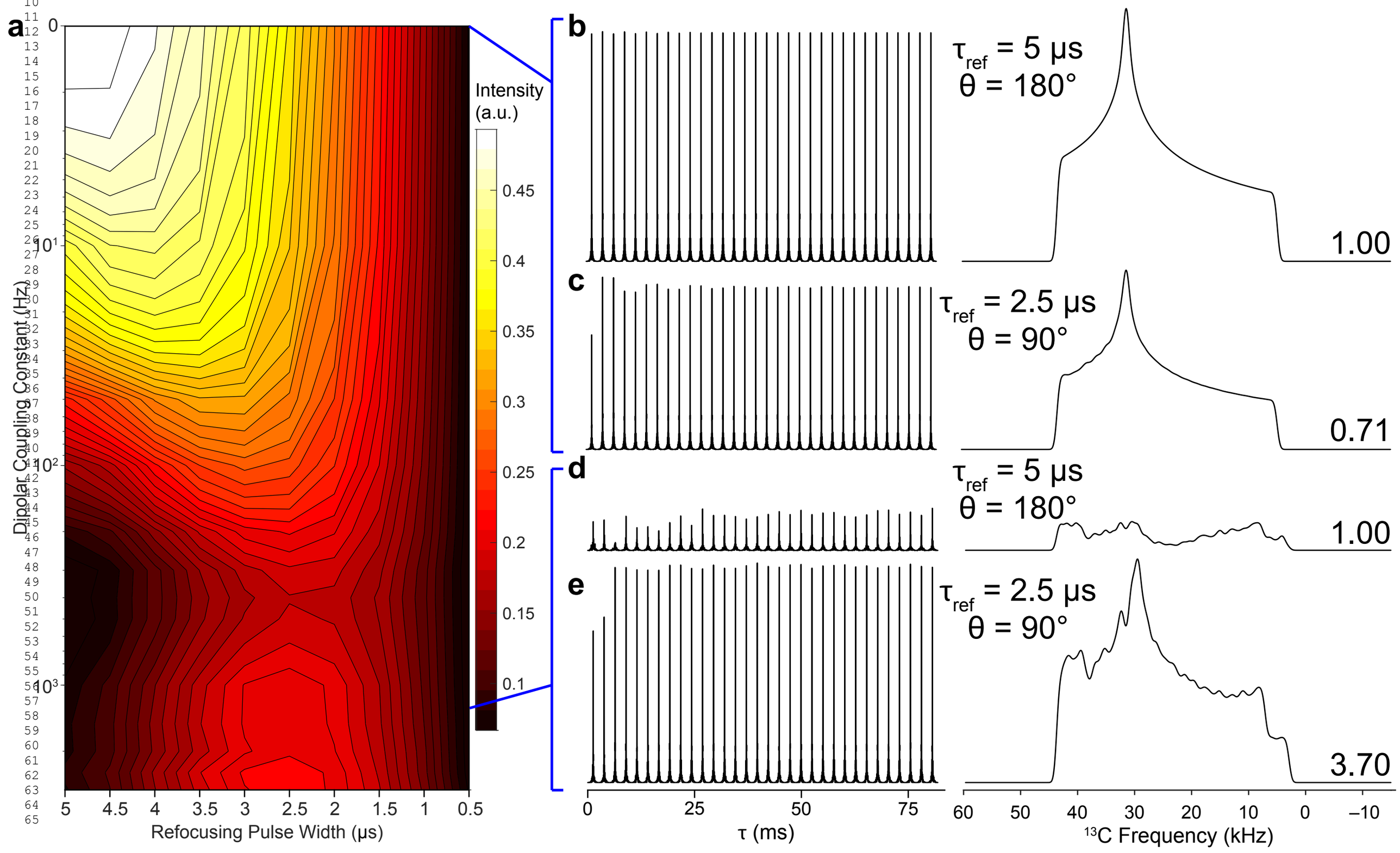
a
b
c
d
e
Intensity (a.u.)
0.45
0.4
0.35
0.3
0.25
0.2
0.15
0.1
0
10¹
10²
10³
Dipolar Coupling Constant (Hz)
5
4.5
4
3.5
3
2.5
2
1.5
1
0.5
Refocusing Pulse Width (μs)
τref = 5 μs
θ = 180°
1.00
τref = 2.5 μs
θ = 90°
0.71
τref = 5 μs
θ = 180°
1.00
τref = 2.5 μs
θ = 90°
3.70
0
25
50
75
τ (ms)
60
50
40
30
20
10
0
–10
13C Frequency (kHz)

Figure 3

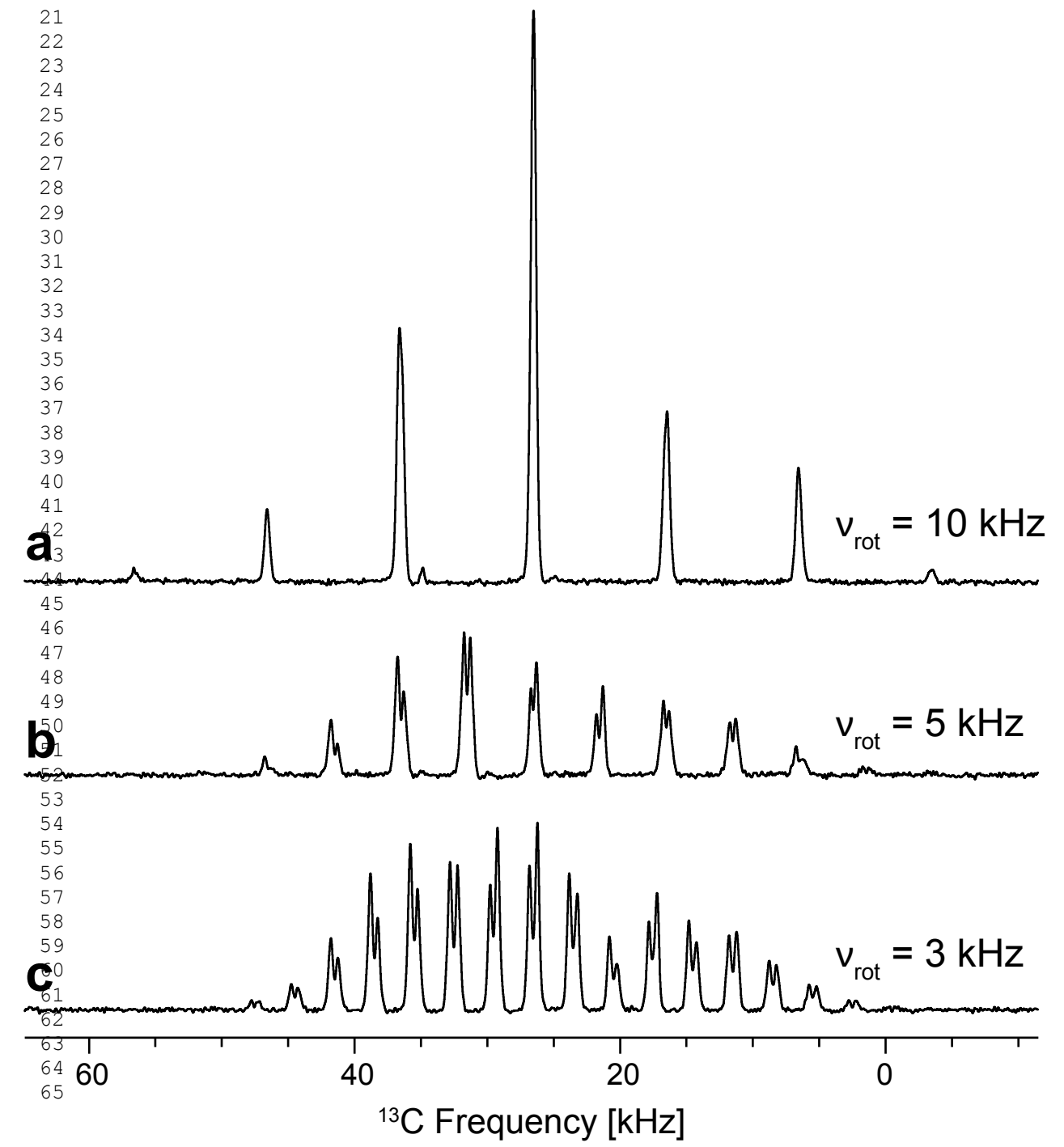
a
ν_{rot} = 10 kHz
b
ν_{rot} = 5 kHz
c
ν_{rot} = 3 kHz
60
40
20
0
^{13}C Frequency [kHz]

Figure 4

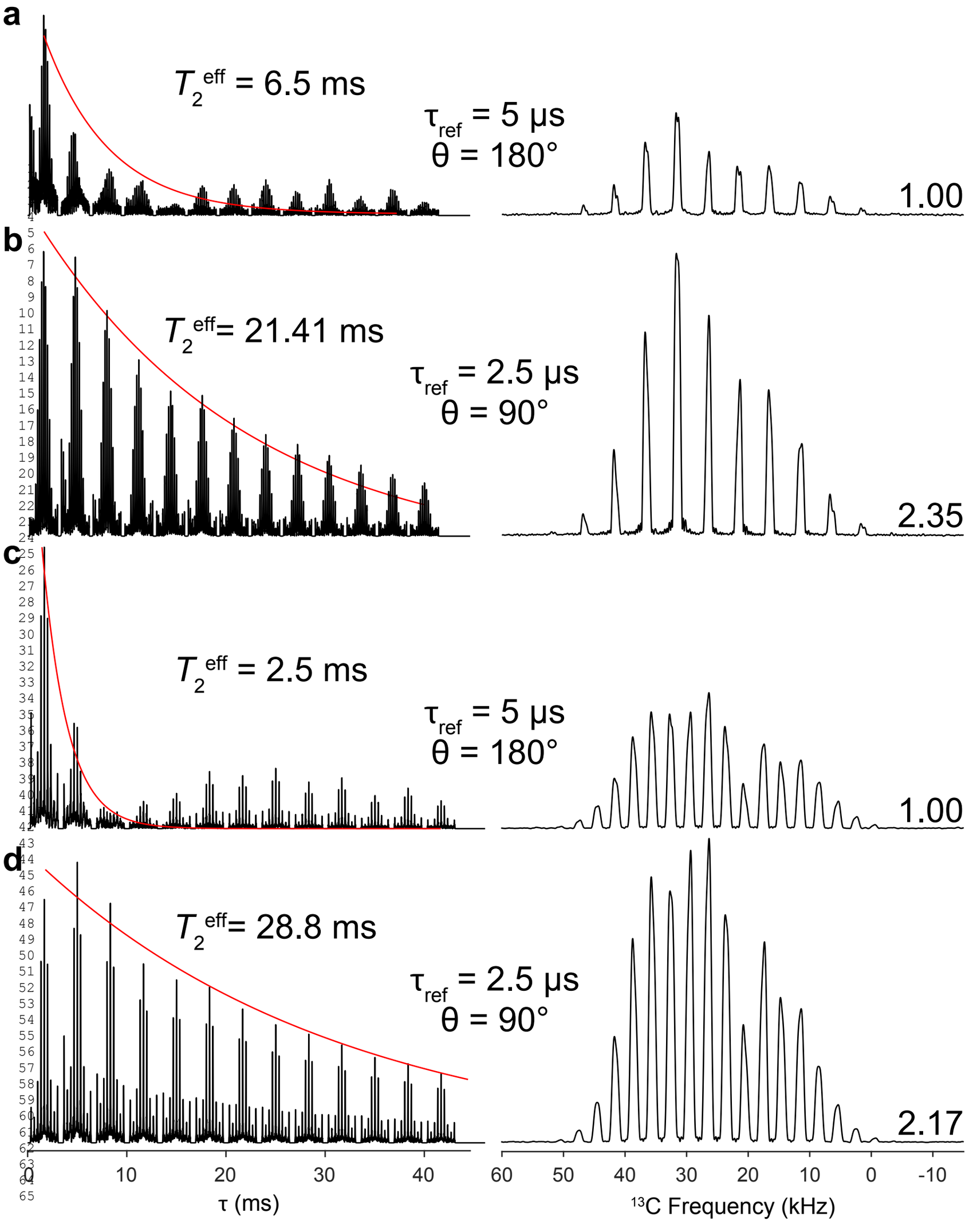
a
T_2^{eff} = 6.5 ms
τ_{ref} = 5 µs
θ = 180°
1.00
b
T_2^{eff}= 21.41 ms
τ_{ref} = 2.5 µs
θ = 90°
2.35
c
T_2^{eff} = 2.5 ms
τ_{ref} = 5 µs
θ = 180°
1.00
d
T_2^{eff}= 28.8 ms
τ_{ref} = 2.5 µs
θ = 90°
2.17
0 10 20 30 40
τ (ms)
60 50 40 30 20 10 0 -10
^{13}C Frequency (kHz)

Figure 5

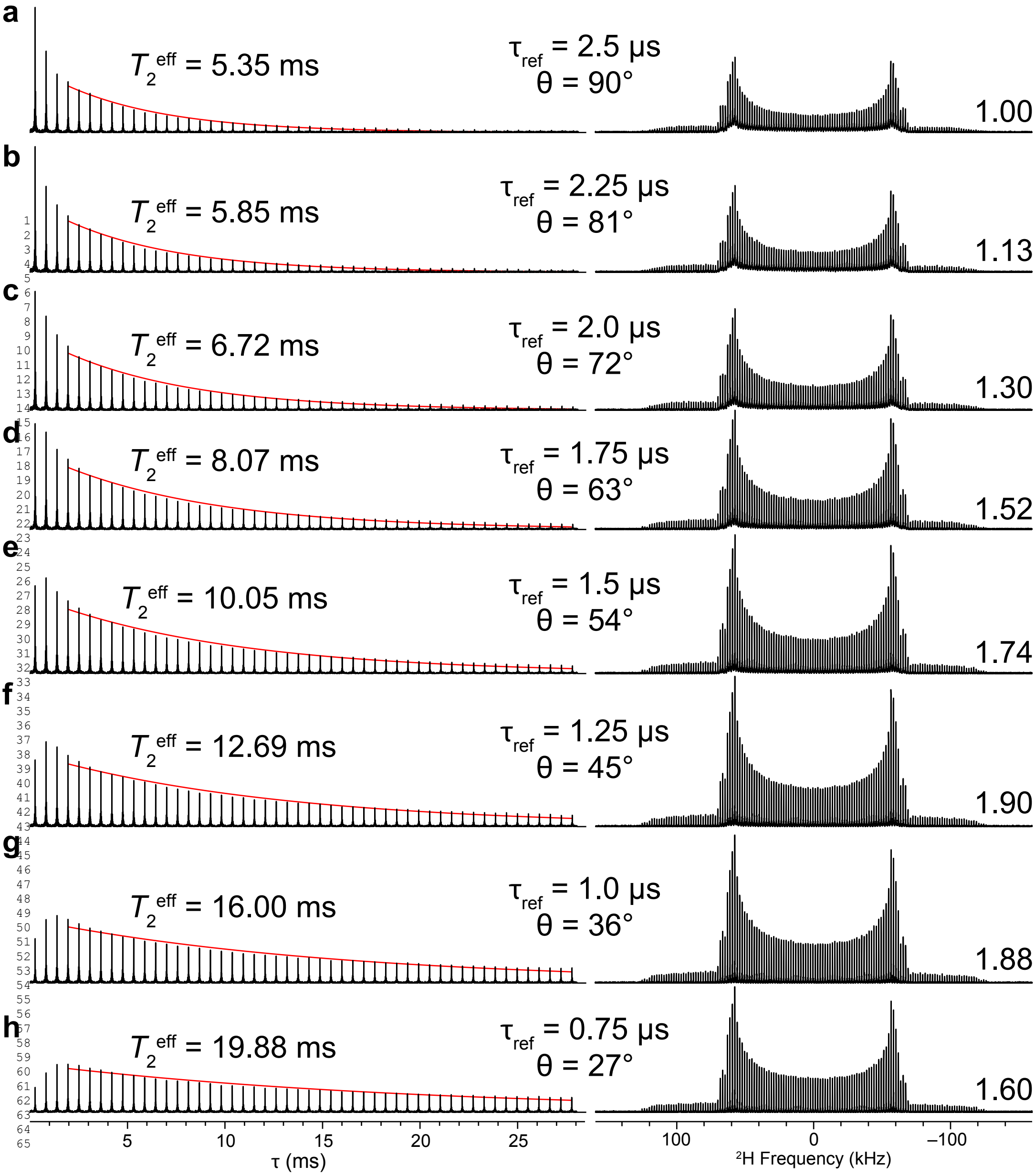
a
T_2^{eff} = 5.35 ms
τ_{ref} = 2.5 µs
θ = 90°
1.00
b
T_2^{eff} = 5.85 ms
τ_{ref} = 2.25 µs
θ = 81°
1.13
c
T_2^{eff} = 6.72 ms
τ_{ref} = 2.0 µs
θ = 72°
1.30
d
T_2^{eff} = 8.07 ms
τ_{ref} = 1.75 µs
θ = 63°
1.52
e
T_2^{eff} = 10.05 ms
τ_{ref} = 1.5 µs
θ = 54°
1.74
f
T_2^{eff} = 12.69 ms
τ_{ref} = 1.25 µs
θ = 45°
1.90
g
T_2^{eff} = 16.00 ms
τ_{ref} = 1.0 µs
θ = 36°
1.88
h
T_2^{eff} = 19.88 ms
τ_{ref} = 0.75 µs
θ = 27°
1.60
5
10
15
20
25
τ (ms)
100
0
–100
^{2}H Frequency (kHz)

Figure 6

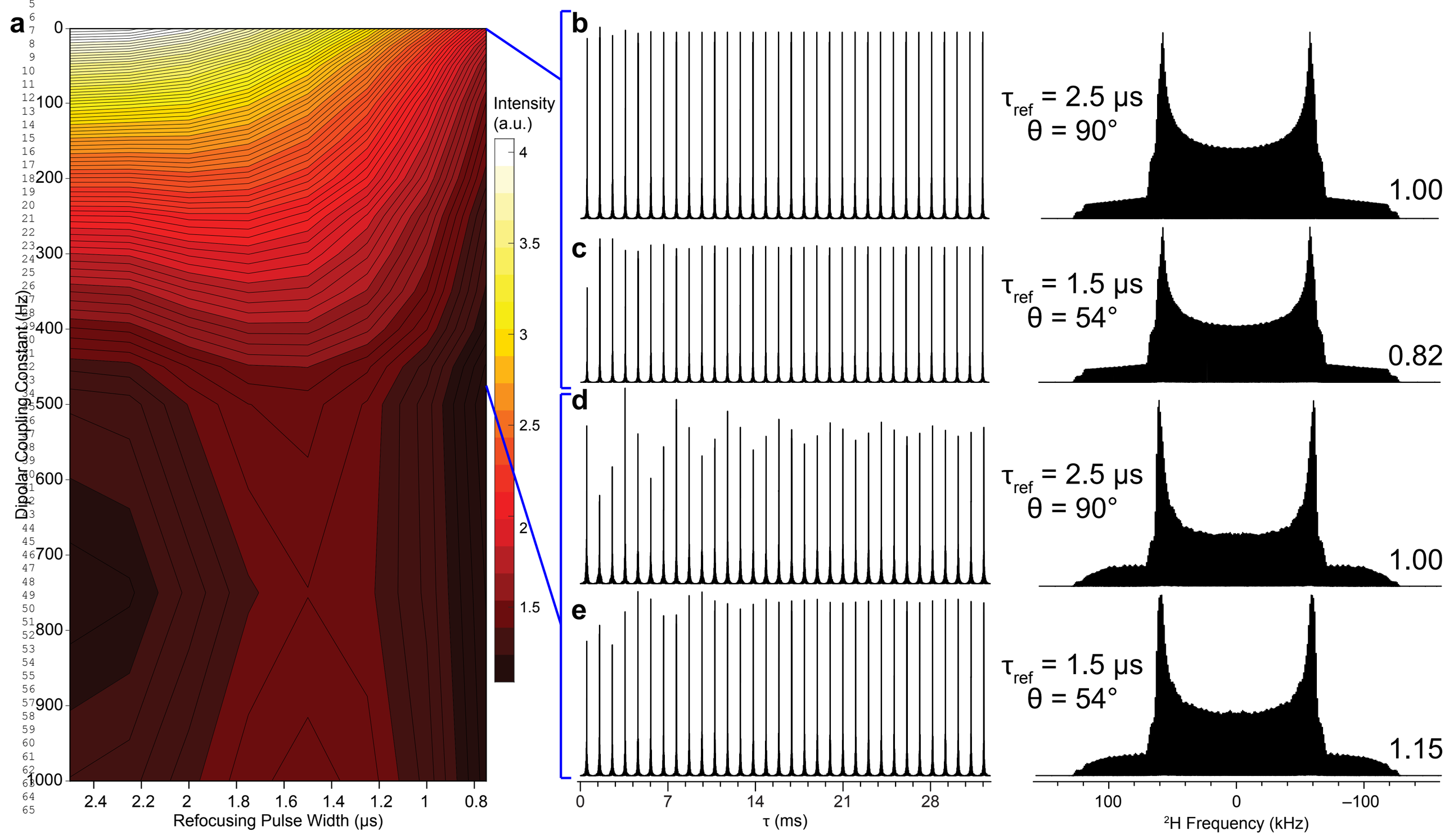
a
b
c
d
e
Intensity (a.u.)
4
3.5
3
2.5
2
1.5
Dipolar Coupling Constant (Hz)
0
100
200
300
400
500
600
700
800
900
1000
2.4
2.2
2
1.8
1.6
1.4
1.2
1
0.8
Refocusing Pulse Width (μs)
τref = 2.5 μs
θ = 90°
1.00
τref = 1.5 μs
θ = 54°
0.82
τref = 2.5 μs
θ = 90°
1.00
τref = 1.5 μs
θ = 54°
1.15
0
7
14
21
28
τ (ms)
100
0
–100
2H Frequency (kHz)

Figure 7

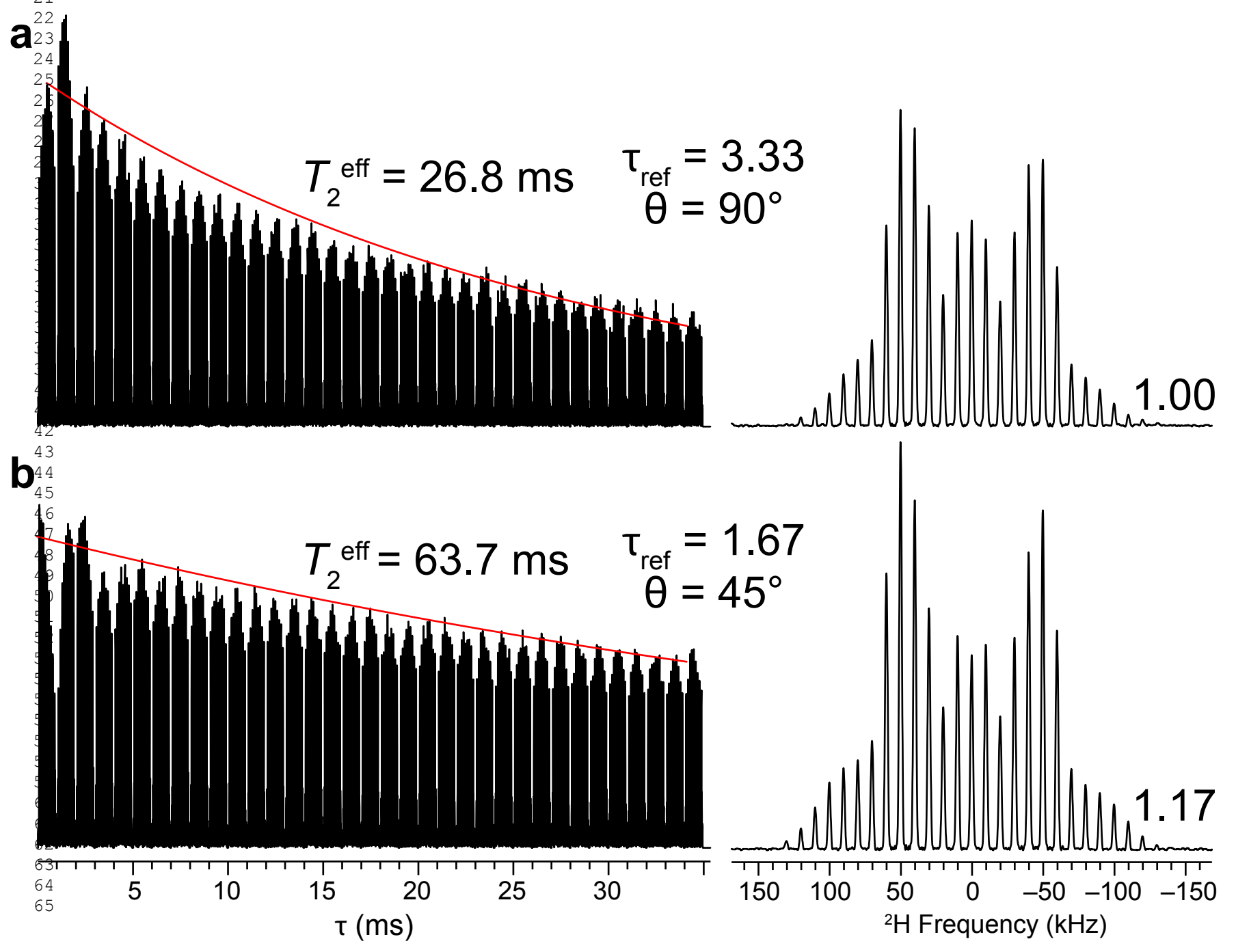
a
T_2^{eff} = 26.8 ms
τ_{ref} = 3.33
θ = 90°
1.00
b
T_2^{eff} = 63.7 ms
τ_{ref} = 1.67
θ = 45°
1.17
5
10
15
20
25
30
τ (ms)
150
100
50
0
–50
–100
–150
²H Frequency (kHz)

Figure 8

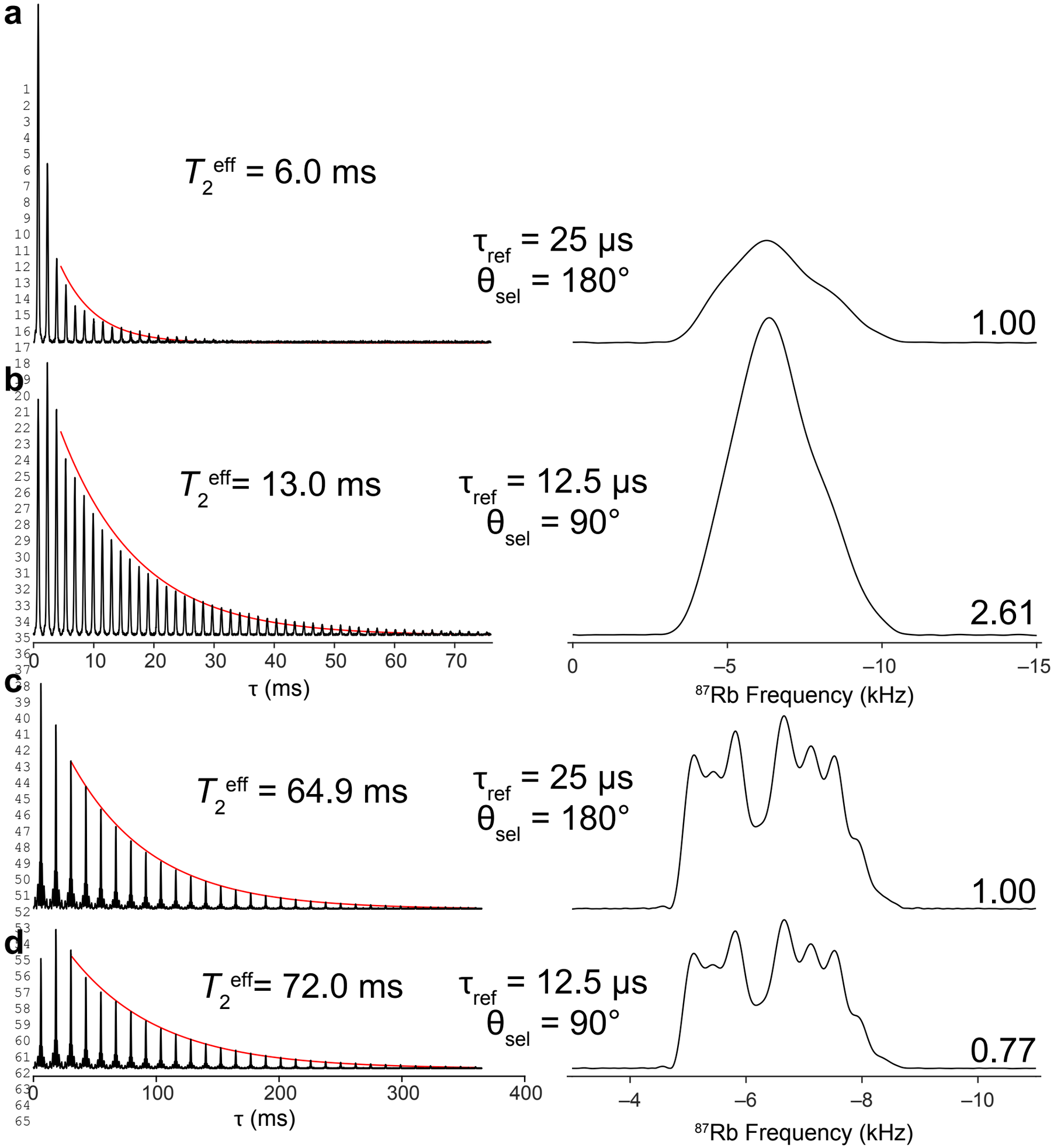
a
T_2^{eff} = 6.0 ms
τ_{ref} = 25 μs
θ_{sel} = 180°
1.00
b
T_2^{eff}= 13.0 ms
τ_{ref} = 12.5 μs
θ_{sel} = 90°
2.61
0 10 20 30 40 50 60 70
τ (ms)
0 –5 –10 –15
^{87}Rb Frequency (kHz)
c
T_2^{eff} = 64.9 ms
τ_{ref} = 25 μs
θ_{sel} = 180°
1.00
d
T_2^{eff}= 72.0 ms
τ_{ref} = 12.5 μs
θ_{sel} = 90°
0.77
0 100 200 300 400
τ (ms)
–4 –6 –8 –10
^{87}Rb Frequency (kHz)

Figure 9

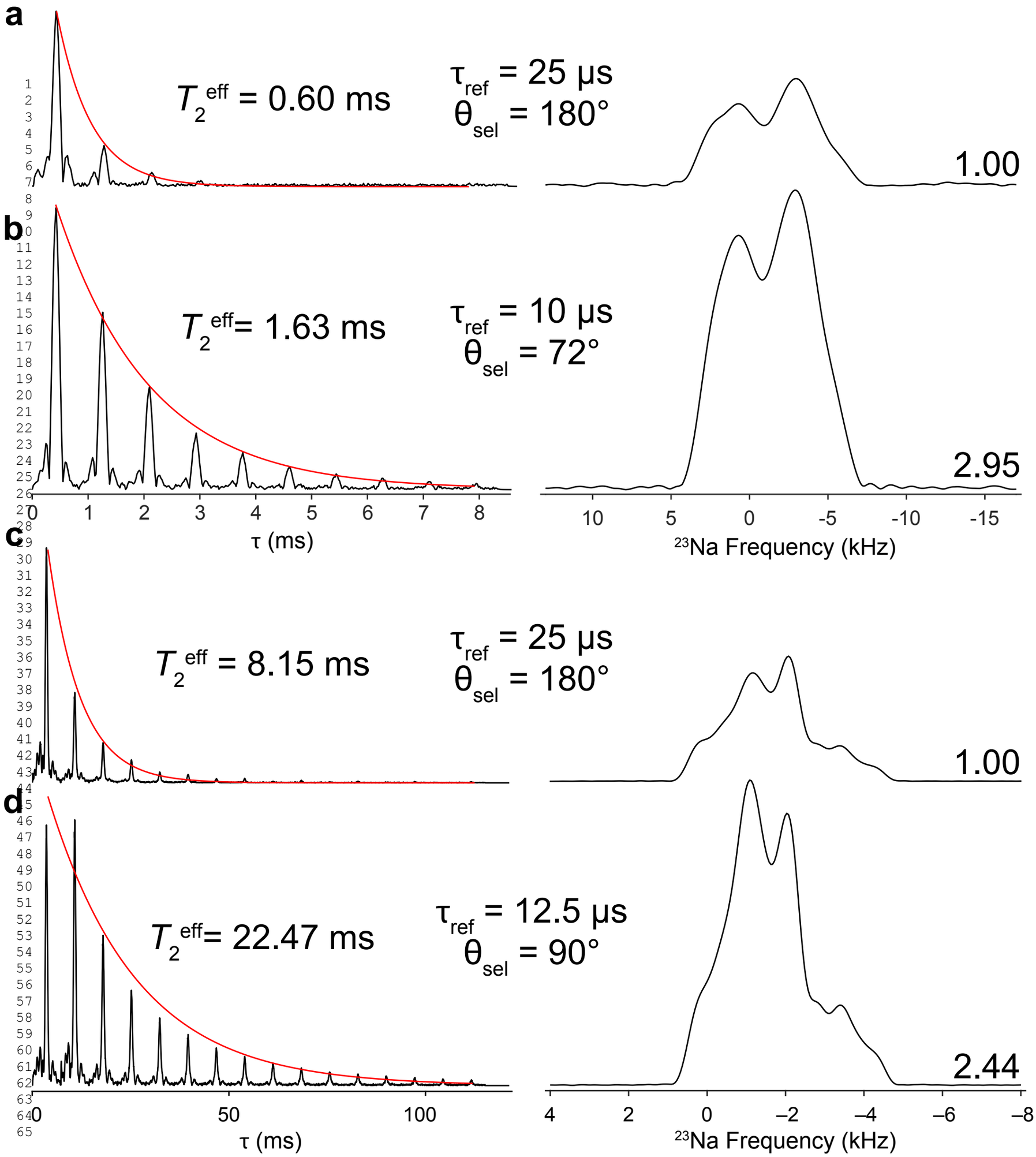
a
T_2^{eff} = 0.60 ms
τ_{ref} = 25 µs
θ_{sel} = 180°
1.00
b
T_2^{eff}= 1.63 ms
τ_{ref} = 10 µs
θ_{sel} = 72°
2.95
0 1 2 3 4 5 6 7 8
τ (ms)
10 5 0 -5 -10 -15
^{23}Na Frequency (kHz)
c
T_2^{eff} = 8.15 ms
τ_{ref} = 25 µs
θ_{sel} = 180°
1.00
d
T_2^{eff}= 22.47 ms
τ_{ref} = 12.5 µs
θ_{sel} = 90°
2.44
0 50 100
τ (ms)
4 2 0 –2 –4 –6 –8
^{23}Na Frequency (kHz)

Figure 10

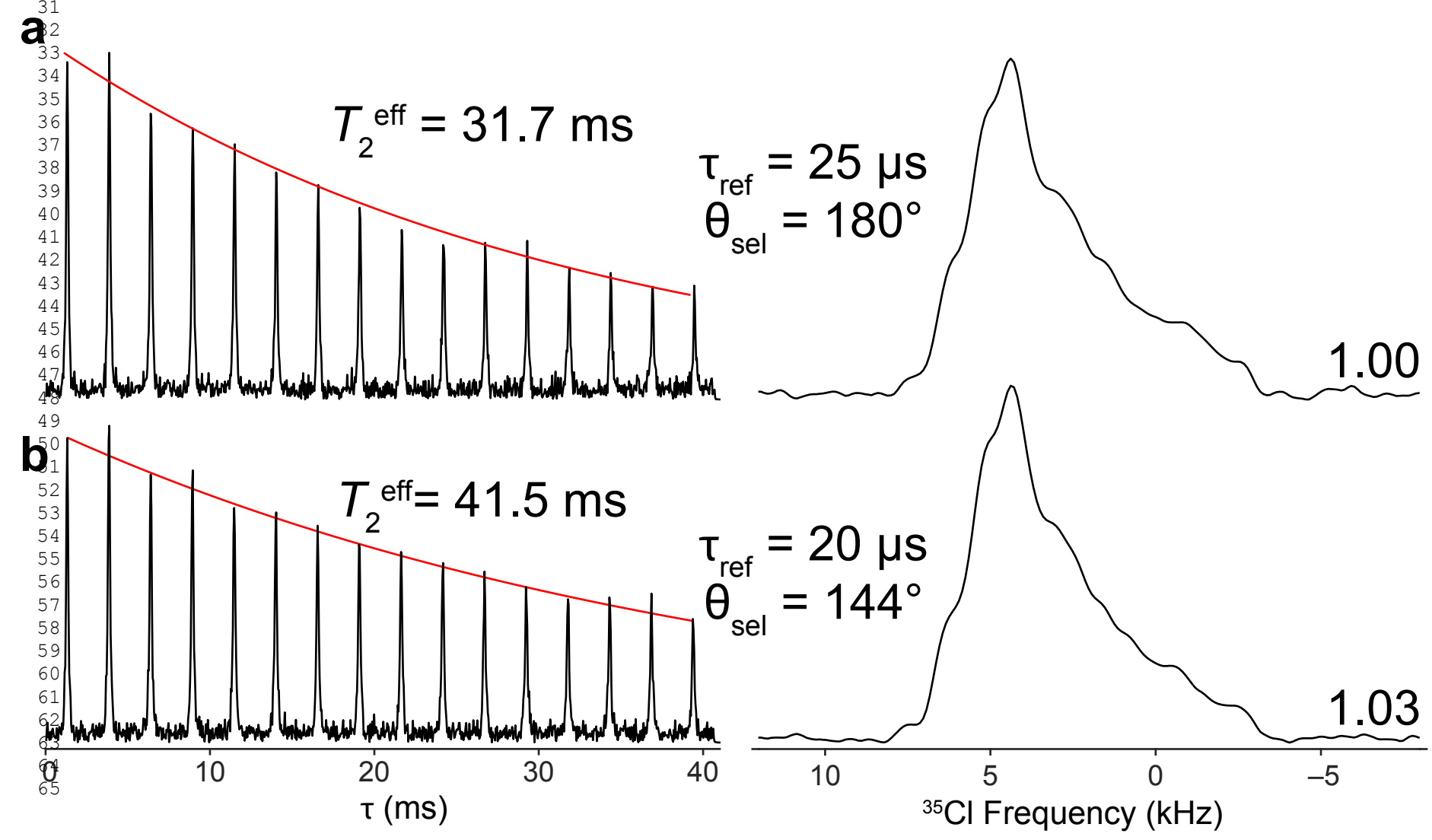
a
T_2^{eff} = 31.7 ms
τ_{ref} = 25 µs
θ_{sel} = 180°
1.00
b
T_2^{eff}= 41.5 ms
τ_{ref} = 20 µs
θ_{sel} = 144°
1.03
0
10
20
30
40
τ (ms)
10
5
0
–5
^{35}Cl Frequency (kHz)

Figure 11

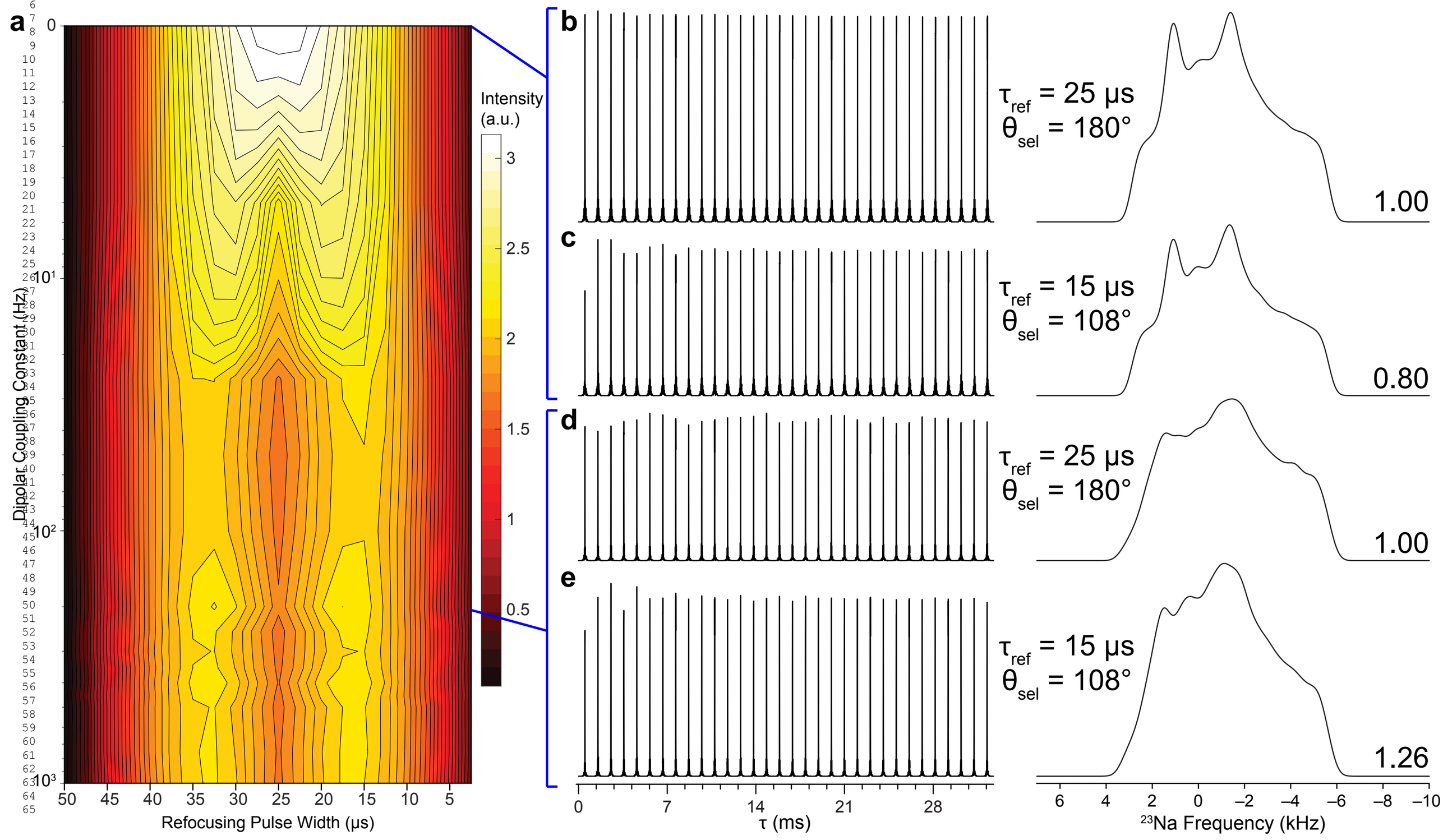
a
b
c
d
e
0
10^1
10^2
10^3
Dipolar Coupling Constant (Hz)
50 45 40 35 30 25 20 15 10 5
Refocusing Pulse Width (μs)
Intensity (a.u.)
3
2.5
2
1.5
1
0.5
τ_{ref} = 25 μs
θ_{sel} = 180°
1.00
τ_{ref} = 15 μs
θ_{sel} = 108°
0.80
τ_{ref} = 25 μs
θ_{sel} = 180°
1.00
τ_{ref} = 15 μs
θ_{sel} = 108°
1.26
0 7 14 21 28
τ (ms)
6 4 2 0 −2 −4 −6 −8 −10
^{23}Na Frequency (kHz)

Supporting Information for

"Reducing the Effects of Weak Homonuclear Dipolar Coupling with CPMG Pulse Sequences for Static and Spinning Solids"

Adam R. Altenhof[1,2], Zhehong Gan[2], and Robert W. Schurko[1,2,*]

1. Department of Chemistry and Biochemistry, Florida State University, Tallahassee, FL, 32310, USA
2. National High Magnetic Field Laboratory, Tallahassee, FL, 32306, USA

*Author to whom correspondence should be addressed.
Phone: (850)-645-8614, E-mail: rschurko@fsu.edu

Table of Contents:

Table S1. Experimental Parameters for ^{1}H-^{13}C CP-CPMG Experiments in **Fig. 1**

	1,2-phthalic anhydride-$^{13}C_2$
Larmor Frequency (MHz)	201.096
Number of Transients	32
Recycle Delay (s)	120.0
Spectral Window (kHz)	200
Dwell Time (μs)	5.0
Spinning Speed, ν_{rot} (kHz)	0
Number of CPMG Loops (*N*)	13
Spin Echo length, τ_{SE} (μs)	1500
^{1}H Excitation Pulse Width (μs)	2.94
^{1}H Excitation Pulse Power (kHz)	85
^{1}H Contact Pulse Power (kHz)	50
^{13}C Contact Pulse Power (kHz)	55.93
^{13}C Refocusing Pulse Amplitude (kHz)	100
^{13}C Refocusing Pulse Width (μs)	5.0 and 2.5
Contact Time (ms)	2.5
^{1}H Decoupling Power (kHz)	50

Table S2. Experimental Parameters for ^{1}H-^{13}C CP/MAS Experiments in **Fig. 3**

	1,2-phthalic anhydride-$^{13}C_2$
Larmor Frequency (MHz)	201.096
Number of Transients	1
Recycle Delay (s)	120.0
Spectral Window (kHz)	200
Dwell Time (μs)	5.0
Spinning Speed, ν_{rot} (kHz)	10, 5, and 3
Pulse Amplitude (kHz)	100
^{1}H Excitation Pulse Width (μs)	2.94
^{1}H Excitation Pulse Power (kHz)	85
^{1}H Contact Pulse Power (kHz)	50
^{13}C Contact Pulse Power (kHz)	33.07, 37.48, and 51.55
Contact Time (ms)	2.5
^{1}H Decoupling Power (kHz)	50

Table S3. Experimental Parameters for ^{1}H-^{13}C CP-CPMG/MAS Experiments in **Fig. 4**

	1,2-phthalic anhydride-$^{13}C_2$
Larmor Frequency (MHz)	201.096
Number of Transients	8
Recycle Delay (s)	120.0
Spectral Window (kHz)	200
Dwell Time (μs)	5.0
Spinning Speed, ν_{rot} (kHz)	5 and 3
Number of CPMG Loops (N)	13
Spin Echo length, τ_{SE} (μs)	2800
^{1}H Excitation Pulse Width (μs)	2.94
^{1}H Excitation Pulse Power (kHz)	85
^{1}H Contact Pulse Power (kHz)	50
^{13}C Contact Pulse Power (kHz)	37.48 and 51.55
^{13}C Refocusing Pulse Amplitude (kHz)	100
^{13}C Refocusing Pulse Width (μs)	5.0 and 2.5
Contact Time (ms)	2.5
^{1}H Decoupling Power (kHz)	50

Table S4. Experimental Parameters for ^{2}H CPMG Experiments in **Fig. 5**

	α-glycine-d_2
Larmor Frequency (MHz)	92.115
Number of Transients	4
Recycle Delay (s)	150.0
Spectral Window (MHz)	1.0
Dwell Time (μs)	1.0
Number of CPMG Loops (N)	50
Spin Echo length, τ_{SE} (μs)	500
Pulse Amplitude (kHz)	100
Excitation Pulse Width, τ_{exc} (μs)	2.5
Refocusing Pulse Width, τ_{ref} (μs)	2.5 to 1.0
^{1}H Decoupling Power (kHz)	50

Table S5. Experimental Parameters for ^{2}H CPMG Experiments in **Fig. S3**

	Urea-d_4
Larmor Frequency (MHz)	92.115
Number of Transients	4
Recycle Delay (s)	600.0
Spectral Window (MHz)	1.0
Dwell Time (μs)	1.0
Number of CPMG Loops (N)	40
Spin Echo length, τ_{SE} (μs)	300
Pulse Amplitude (kHz)	100
Excitation Pulse Width, τ_{exc} (μs)	2.5
Refocusing Pulse Width, τ_{ref} (μs)	2.5 and 1.25
^{1}H Decoupling Power (kHz)	0

Table S6. Experimental Parameters for ^{2}H CPMG Experiments in **Fig. S4**

	DMNAP-d_{12}
Larmor Frequency (MHz)	92.115
Number of Transients	128
Recycle Delay (s)	1.0
Spectral Window (MHz)	1.0
Dwell Time (μs)	1.0
Number of CPMG Loops (N)	40
Spin Echo length, τ_{SE} (μs)	700
Pulse Amplitude (kHz)	100
Excitation Pulse Width, τ_{exc} (μs)	2.5
Refocusing Pulse Width, τ_{ref} (μs)	2.5, 1.25, and 1.00
^{1}H Decoupling Power (kHz)	0

Table S7. Experimental Parameters for ^{2}H CPMG Experiments in **Fig. S5**

	Benzoic Acid-d
Larmor Frequency (MHz)	92.115
Number of Transients	8
Recycle Delay (s)	8.0
Spectral Window (MHz)	1.0
Dwell Time (μs)	1.0
Number of CPMG Loops (N)	120
Spin Echo length, τ_{SE} (μs)	300
Pulse Amplitude (kHz)	100
Excitation Pulse Width, τ_{exc} (μs)	2.5
Refocusing Pulse Width, τ_{ref} (μs)	2.5 and 1.25
^{1}H Decoupling Power (kHz)	50

Table S8. Experimental Parameters for ^{2}H CPMG Experiments in **Fig. S6**

	MIL-53-d_4
Larmor Frequency (MHz)	92.115
Number of Transients	8
Recycle Delay (s)	140.0
Spectral Window (MHz)	1.0
Dwell Time (μs)	1.0
Number of CPMG Loops (N)	50
Spin Echo length, τ_{SE} (μs)	300
Pulse Amplitude (kHz)	100
Excitation Pulse Width, τ_{exc} (μs)	2.5
Refocusing Pulse Width, τ_{ref} (μs)	2.5 and 1.25
^{1}H Decoupling Power (kHz)	50

Table S9. Experimental Parameters for ^{2}H CPMG Experiments in **Fig. S7**

	Dimedone-d
Larmor Frequency (MHz)	92.115
Number of Transients	4
Recycle Delay (s)	100.0
Spectral Window (MHz)	1.0
Dwell Time (μs)	1.0
Number of CPMG Loops (N)	120
Spin Echo length, τ_{SE} (μs)	300
Pulse Amplitude (kHz)	100
Excitation Pulse Width, τ_{exc} (μs)	2.5
Refocusing Pulse Width, τ_{ref} (μs)	2.5 and 1.25
^{1}H Decoupling Power (kHz)	50

Table S10. Experimental Parameters for ^{2}H CPMG/MAS Experiments in **Fig. 7**

	α-glycine-d_2
Larmor Frequency (MHz)	61.415
Number of Transients	1
Recycle Delay (s)	70.0
Spectral Window (MHz)	1.0
Dwell Time (μs)	1.0
Number of CPMG Loops (N)	50
Spin Echo length, τ_{SE} (μs)	935
Spinning Speed, ν_{rot} (kHz)	10
Rotor Period, τ_{rot} (μs)	100
Pulse Amplitude (kHz)	75
Excitation Pulse Width, τ_{exc} (μs)	3.33
Refocusing Pulse Width, τ_{ref} (μs)	3.33 and 1.67
^{1}H Decoupling Power (kHz)	40

Table S11. Experimental Parameters for ^{87}Rb Experiments in **Fig. 8**

	$RbNO_3$
Larmor Frequency (MHz)	196.348
Number of Transients	16
Recycle Delay (s)	0.5
Spectral Window (kHz)	20
Dwell Time (μs)	40
Spinning Speed, ν_{rot} (kHz)	0 and 10
Number of CPMG Loops (N)	50 and 30
Spin Echo length, τ_{SE} (ms)	1.5 and 12
Pulse Amplitude (kHz)	10
Excitation Pulse Width, τ_{exc} (μs)	25
Refocusing Pulse Width, τ_{ref} (μs)	25 and 12.5

Table S12. Experimental Parameters for ^{23}Na Experiments in **Fig. 9**

	Na_2SO_4
Larmor Frequency (MHz)	158.73
Number of Transients	8 and 16
Recycle Delay (s)	30
Spectral Window (kHz)	100 and 20
Dwell Time (μs)	10 and 40
Spinning Speed, ν_{rot} (kHz)	0 and 10
Number of CPMG Loops (N)	10 and 16
Spin Echo length, τ_{SE} (ms)	0.8 and 7
Pulse Amplitude (kHz)	10
Excitation Pulse Width, τ_{exc} (μs)	25
Refocusing Pulse Width, τ_{ref} (μs)	25, 12.5, and 10

Table S13. Experimental Parameters for ^{35}Cl Experiments in **Fig. 10**

	L-Histidine $HCl \cdot H_2O$
Larmor Frequency (MHz)	158.73
Number of Transients	16
Recycle Delay (s)	10
Spectral Window (kHz)	50
Dwell Time (μs)	20
Spinning Speed, ν_{rot} (kHz)	0
Number of CPMG Loops (N)	16
Spin Echo length, τ_{SE} (ms)	2.5
Pulse Amplitude (kHz)	10
Excitation Pulse Width, τ_{exc} (μs)	25
Refocusing Pulse Width, τ_{ref} (μs)	25 and 20

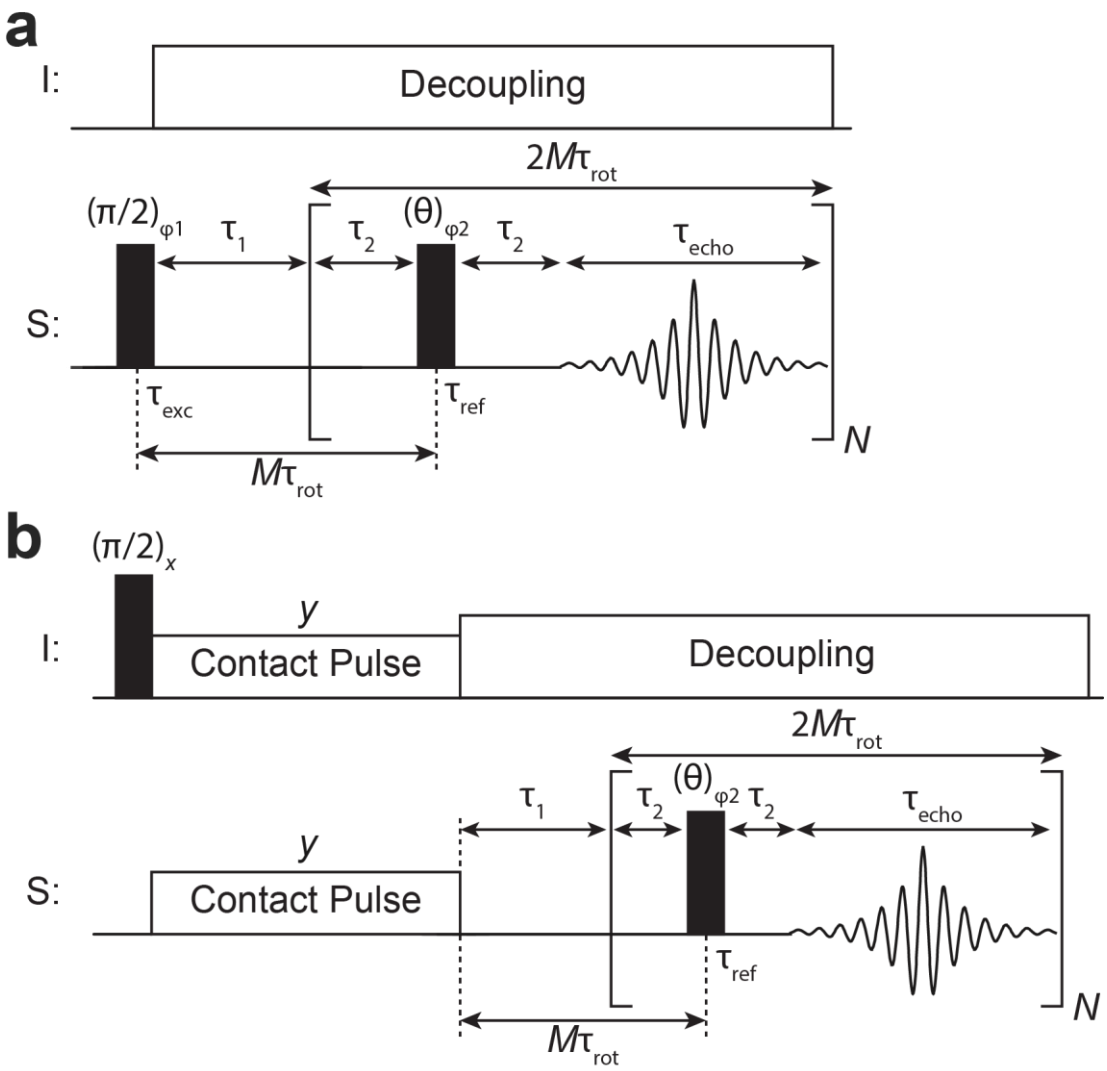

Figure S1: (a) The (Q)CPMG and (b) CP-(Q)CPMG pulse sequences used throughout this work. θ is the flip angle of the refocusing pulse that has an RF amplitude of ν_1 and a pulse width of τ_{ref}. For $I = 3/2$ nuclei in this work, the refocusing pulse widths are scaled by 1/2 to give central-transition selective pulses with flip angle θ_{sel}. φ_1 and φ_2 denote 8-step and 16-step phase cycling schemes in (a) and (b), respectively, as detailed by Iijima *et al.*[1,2] The sequences are used under static and MAS conditions, the latter of which requires rotor-synchronization with the condition $2M\tau_{rot} = 2\tau_2 + \tau_{ref} + \tau_{echo}$ where $(2M–1)$ rotational echoes are encoded in each spin echo and M is an integer.[3]

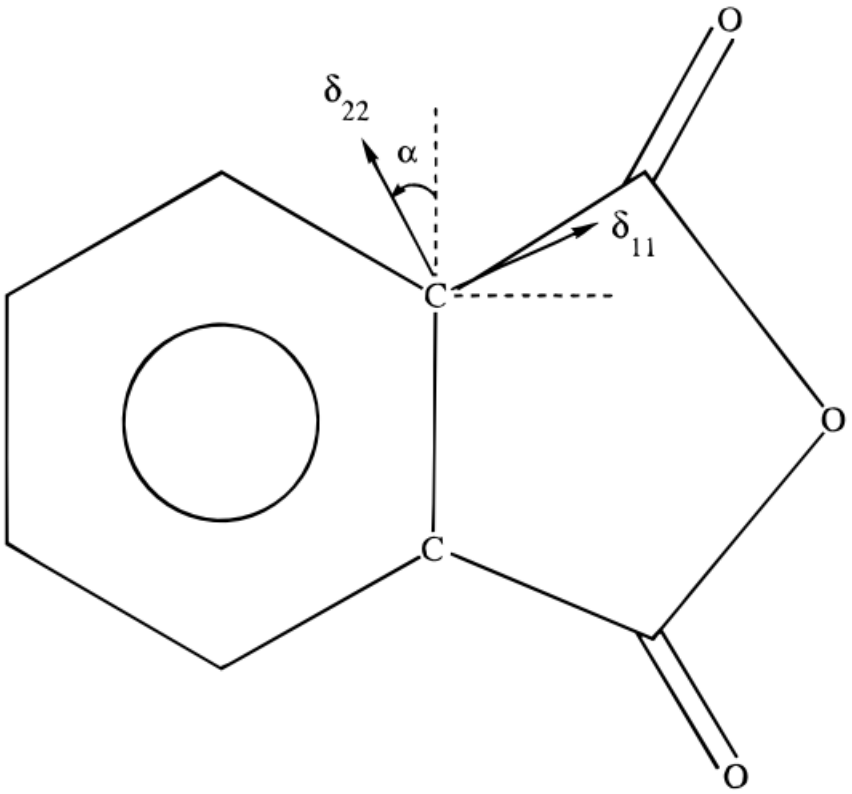

Figure S2: Orientation of the principal axis system of the carbon chemical shift tensor in phthalic anhydride-1,2-$^{13}C_2$. Figure adapted from reference 4.

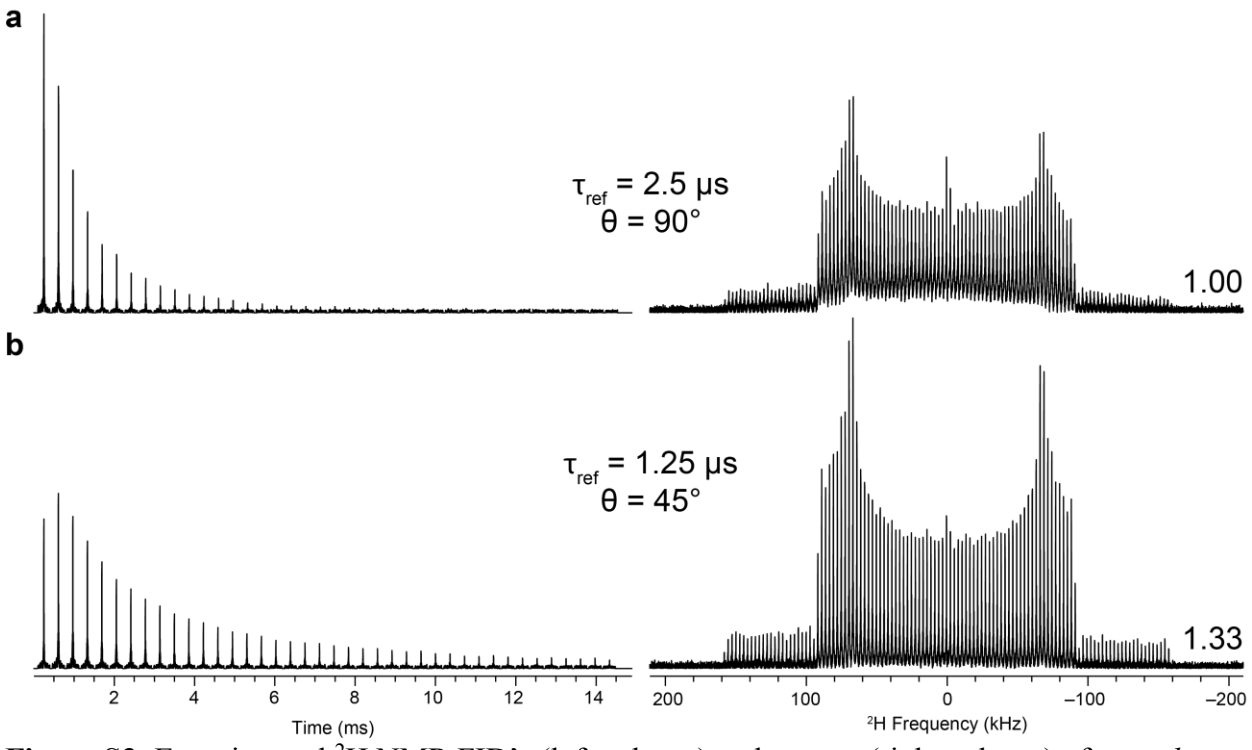

Figure S3: Experimental ^{2}H NMR FID's (left column) and spectra (right column) of urea-d_4 acquired with a CPMG pulse sequence using excitation and refocusing pulse amplitudes of 100 kHz, an excitation pulse width of 2.5 μs, and refocusing pulse widths of (a) 2.5 μs (90°) and (b) 1.25 μs (45°). In each case the integral of the powder pattern is displayed to the right of the pattern and is normalized with respect to the pattern in (a).

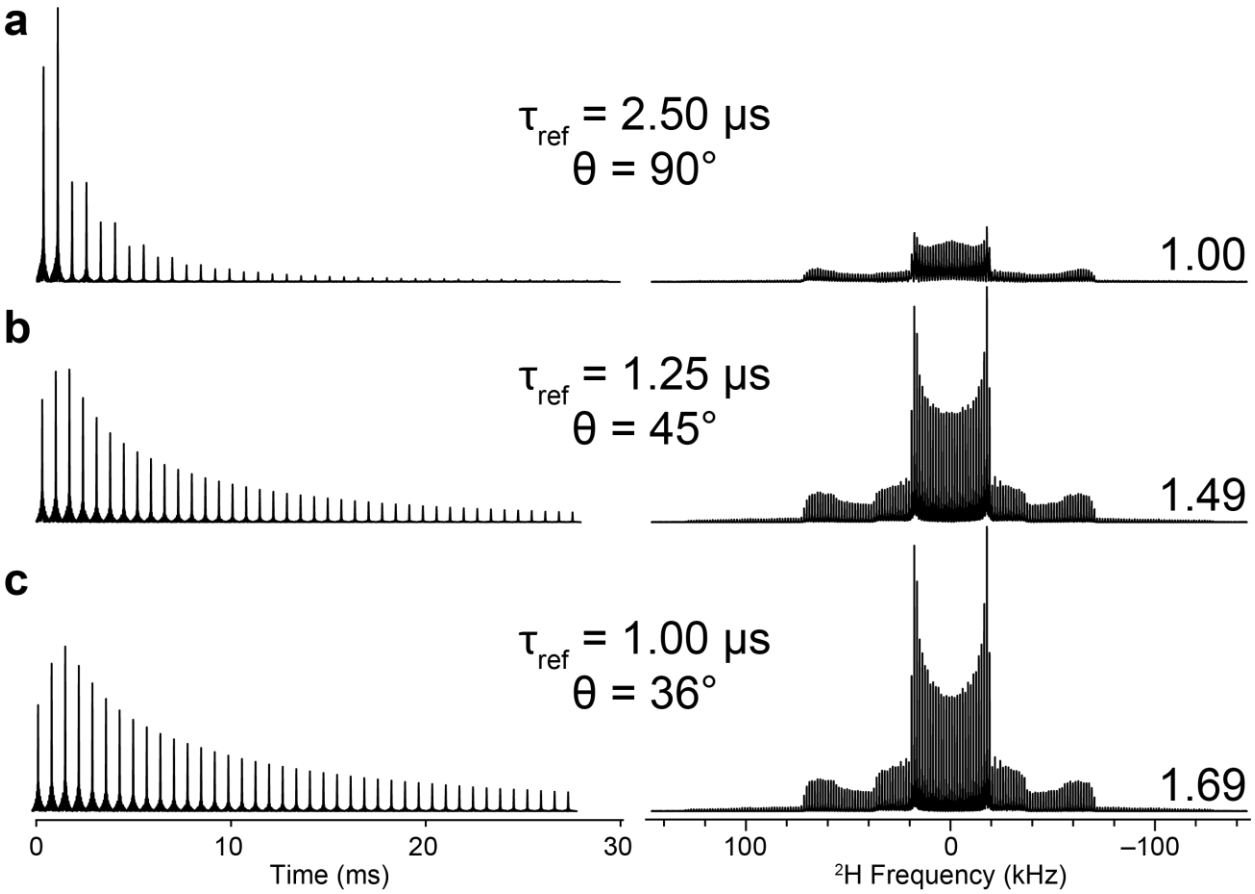

Figure S4: Experimental ^{2}H NMR FID's (left column) and spectra (right column) of DMNAP-d_{12} acquired with a CPMG pulse sequence using excitation and refocusing pulse amplitudes of 100 kHz, an excitation pulse width of 2.5 μs, and refocusing pulse widths of (a) 2.5 μs (90°), (b) 1.25 μs (45°), and 1.00 μs (36°). In each case the integral of the powder pattern is displayed to the right of the pattern and is normalized with respect to the pattern in (a).

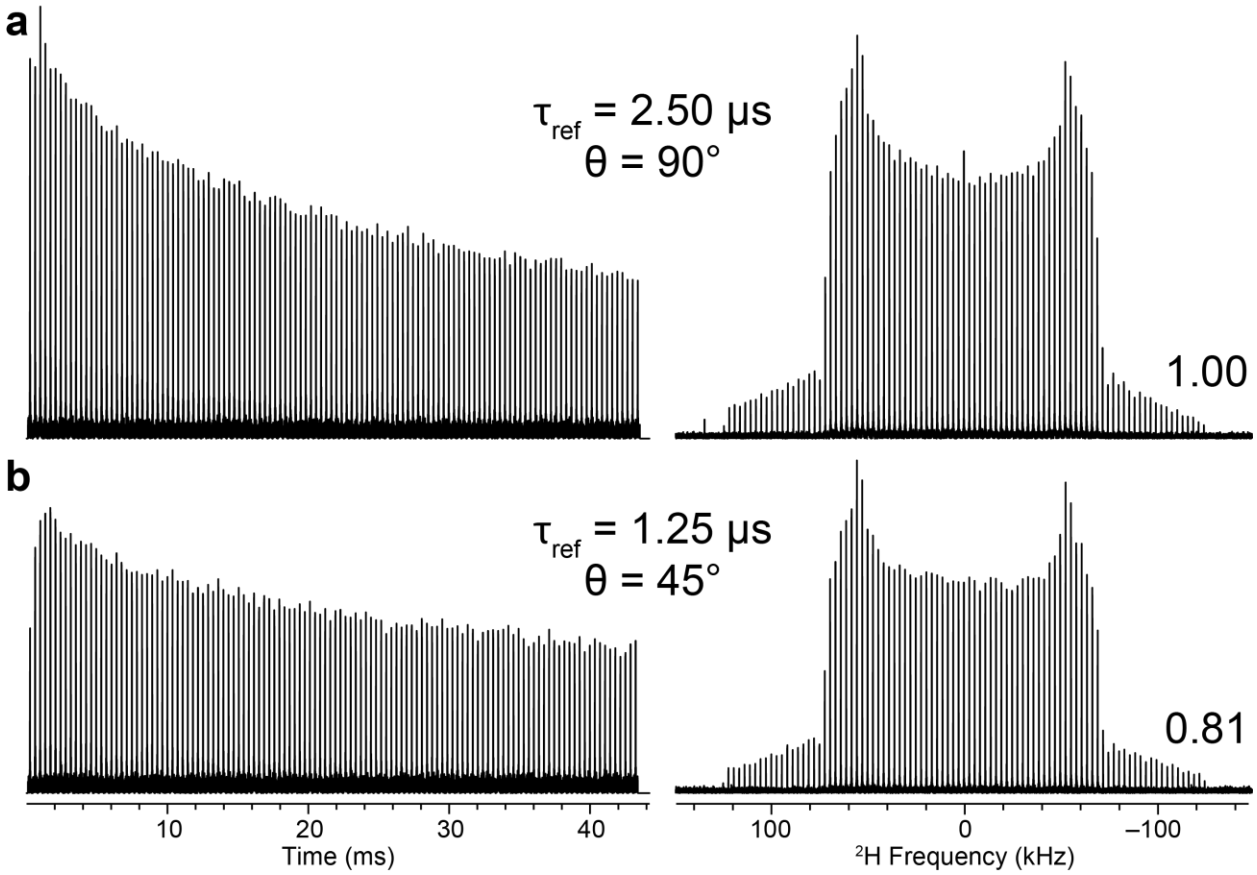

Figure S5: Experimental ^{2}H NMR FID's (left column) and spectra (right column) of benzoic acid-*d* acquired with a CPMG pulse sequence using excitation and refocusing pulse amplitudes of 100 kHz, an excitation pulse width of 2.5 µs, and refocusing pulse widths of (a) 2.5 µs (90°) and (b) 1.25 µs (45°). In each case the integral of the powder pattern is displayed to the right of the pattern and is normalized with respect to the pattern in (a).

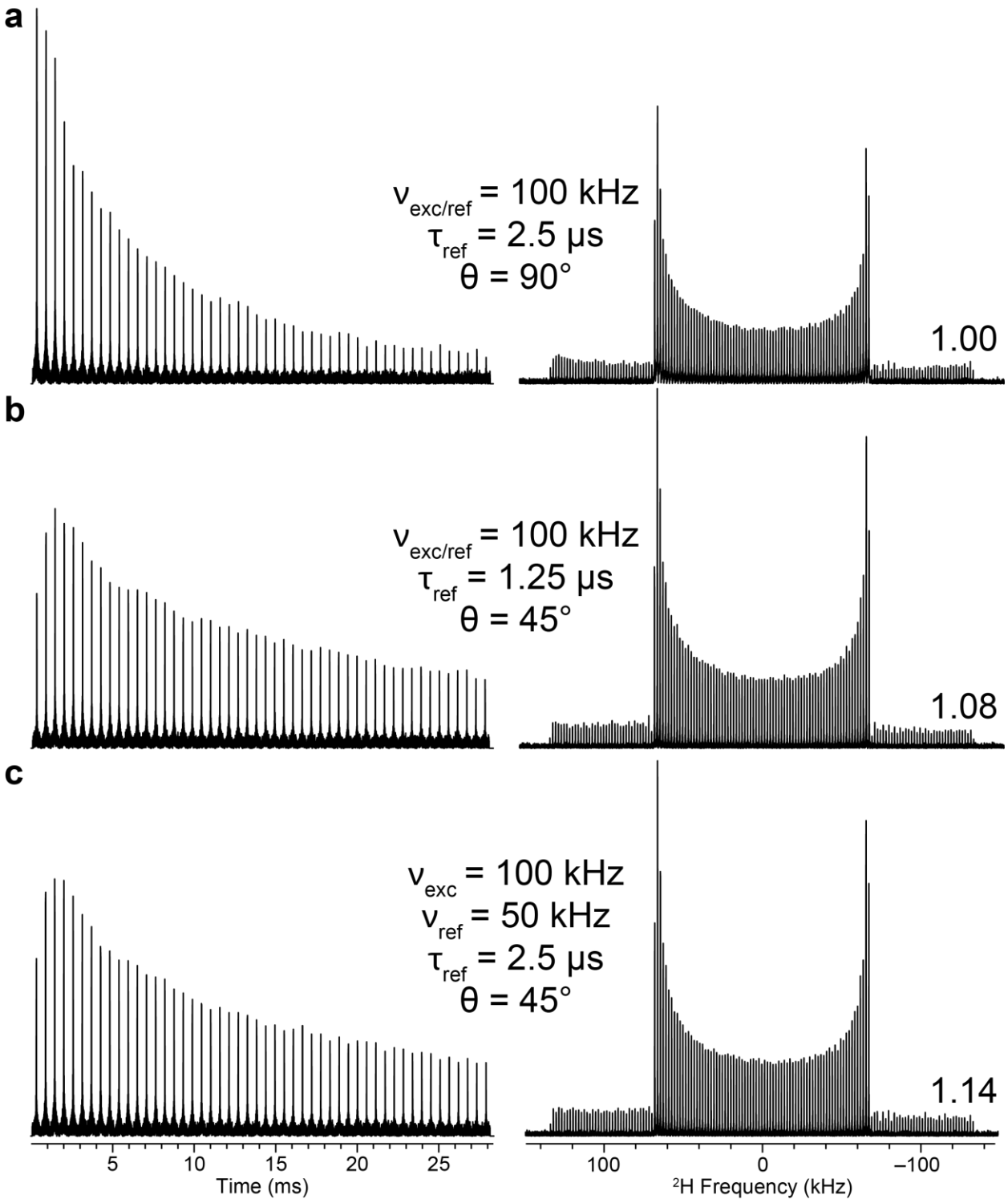

Figure S6: ^{2}H NMR of MIL-53-d_4 with the time-domain spin-echo trains in the left column and the spectra in the right column. Signal is acquired with a CPMG pulse sequence using excitation and refocusing pulse amplitudes of 100 kHz, an excitation pulse width of 2.5 μs, and refocusing pulse widths of (a) 2.5 μs (90°) and (b) 1.25 μs (45°), and (c) refocusing pulse amplitudes of 50 kHz and pulse widths of 2.5 μs (45°). In every case the integral of the powder pattern is displayed to the right of the pattern and is normalized with respect to the pattern in (a).

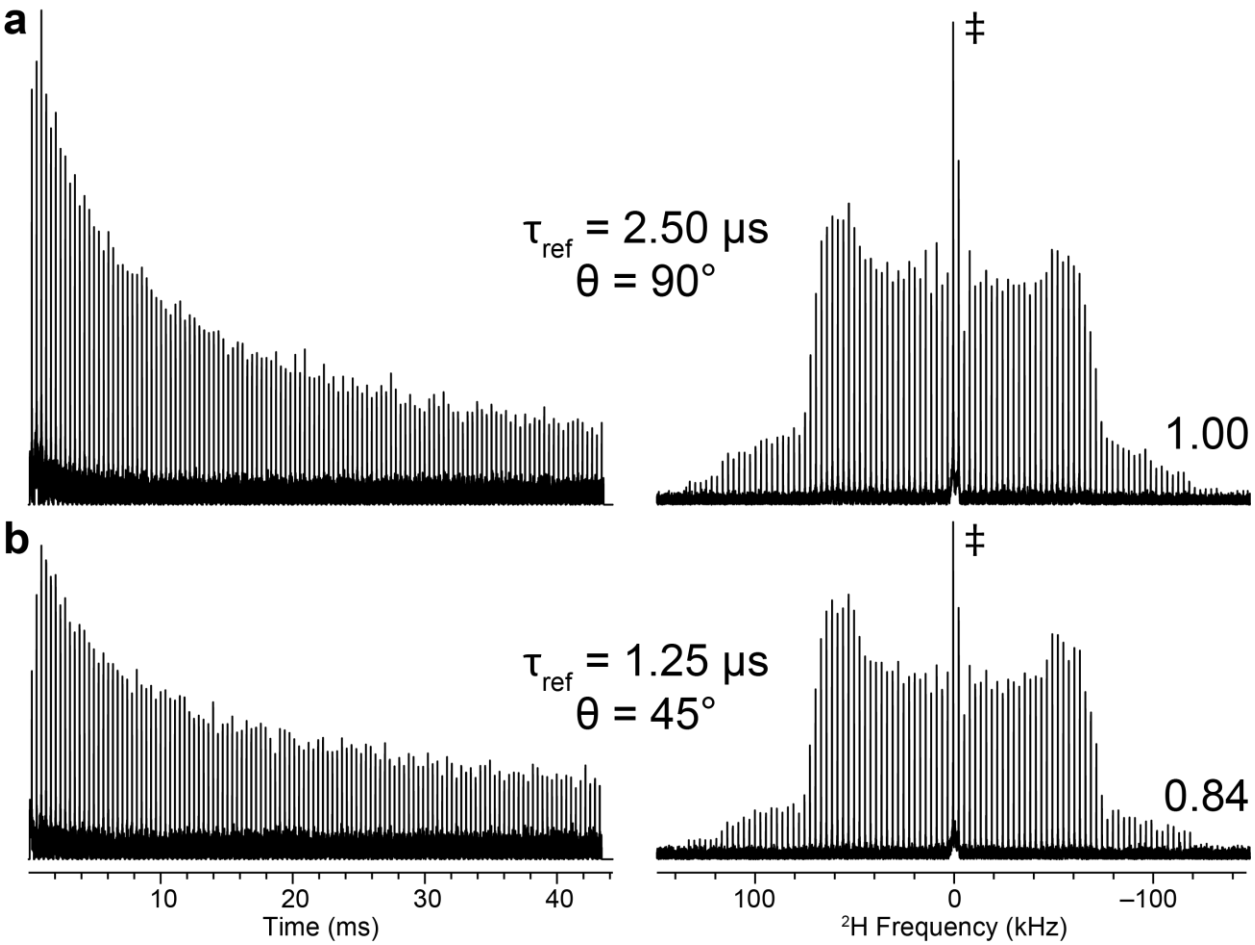

Figure S7: ^{2}H NMR of dimedone-*d* with the time-domain spin-echo trains in the left column and the spectra in the right column. Signal is acquired with a CPMG pulse sequence using excitation and refocusing pulse amplitude of 100 kHz, an excitation pulse width of 2.5 μs, and refocusing pulse widths of (a) 2.5 μs (90°) and (b) 1.25 μs (45°). ‡ denotes residual D_2O signal from the synthesis. In each case the integral of the powder pattern is displayed to the right of the pattern and is normalized with respect to the pattern in (a).

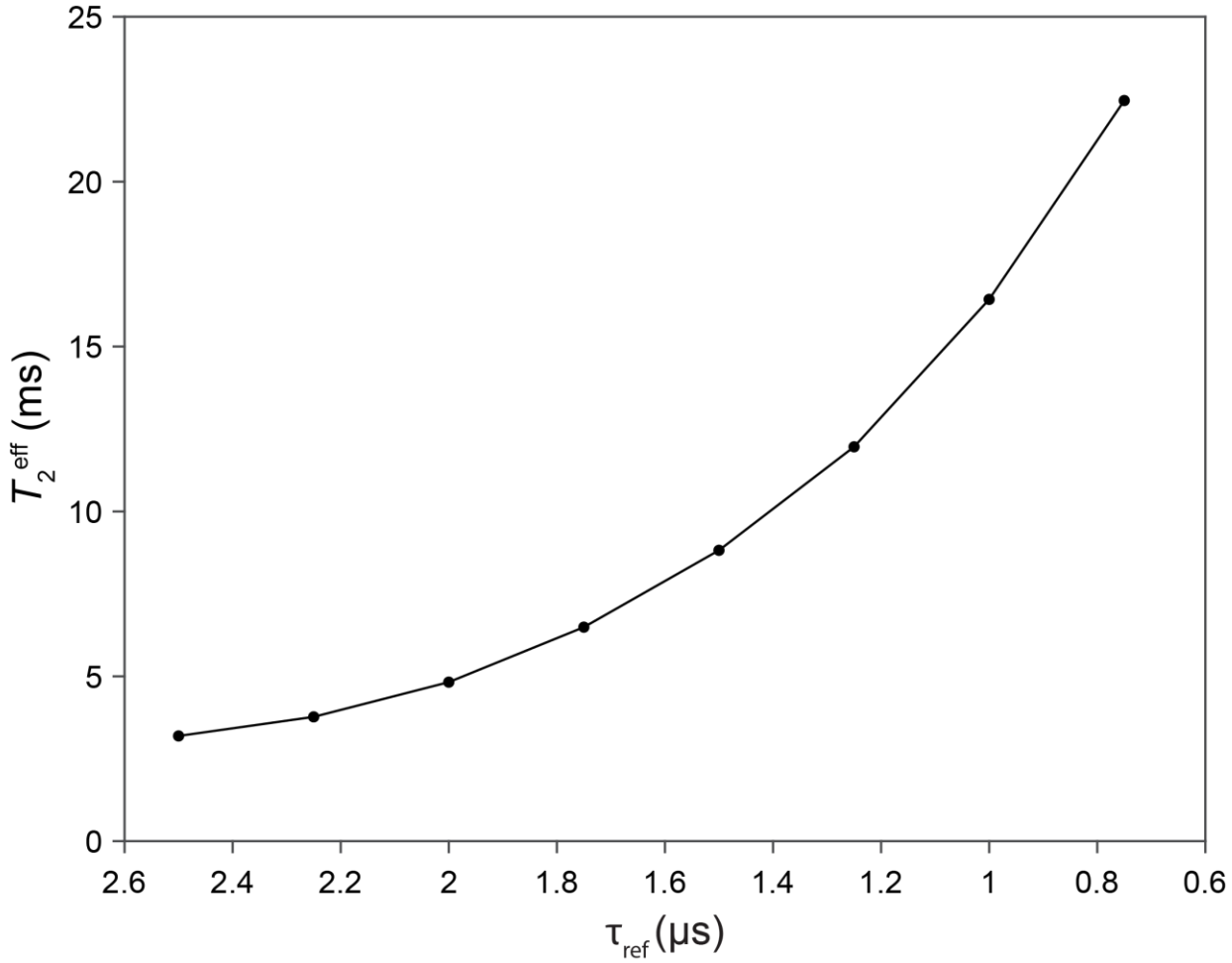

Figure S8: Monoexponential T_2^{eff} fits for ^{2}H NMR FID's of α-glycine-d_2 as a function of refocusing pulse width, τ_{ref}, corresponding to data shown in **Figure 5**.

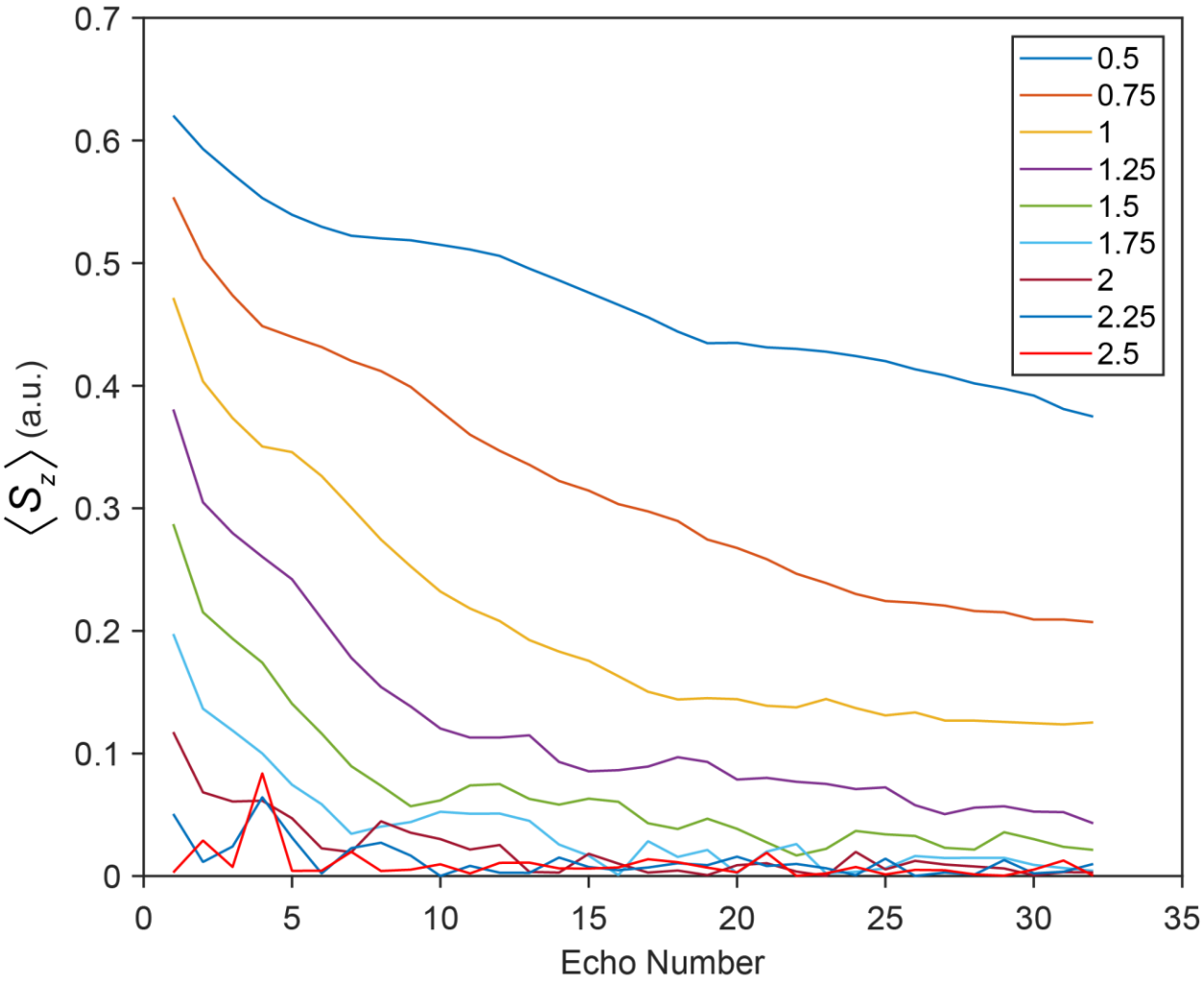

Figure S9: $\langle S_z \rangle$ (zero-quantum coherence, ZQC) calculated for a single point immediately after the refocusing pulses for a CPMG pulse sequence that uses RF amplitudes of 100 kHz, an excitation pulse of 2.5 μs, and refocusing pulse widths, τ_{ref}, that vary from 2.5 to 0.5 μs according to the legend. The ^{2}H spin system is simulated as described for **Figure 6** with a dipolar coupling of 450 Hz. A pulse with $\tau_{ref} = 2.5$ μs creates no ZQC after the first echo and only negligible amounts afterwards. Shorter refocusing pulses generate ZQCs of greater magnitude, which can increase T_2^{eff} and cause an initial build-up of spin polarization in the first few spin echoes observed in a CPMG train.

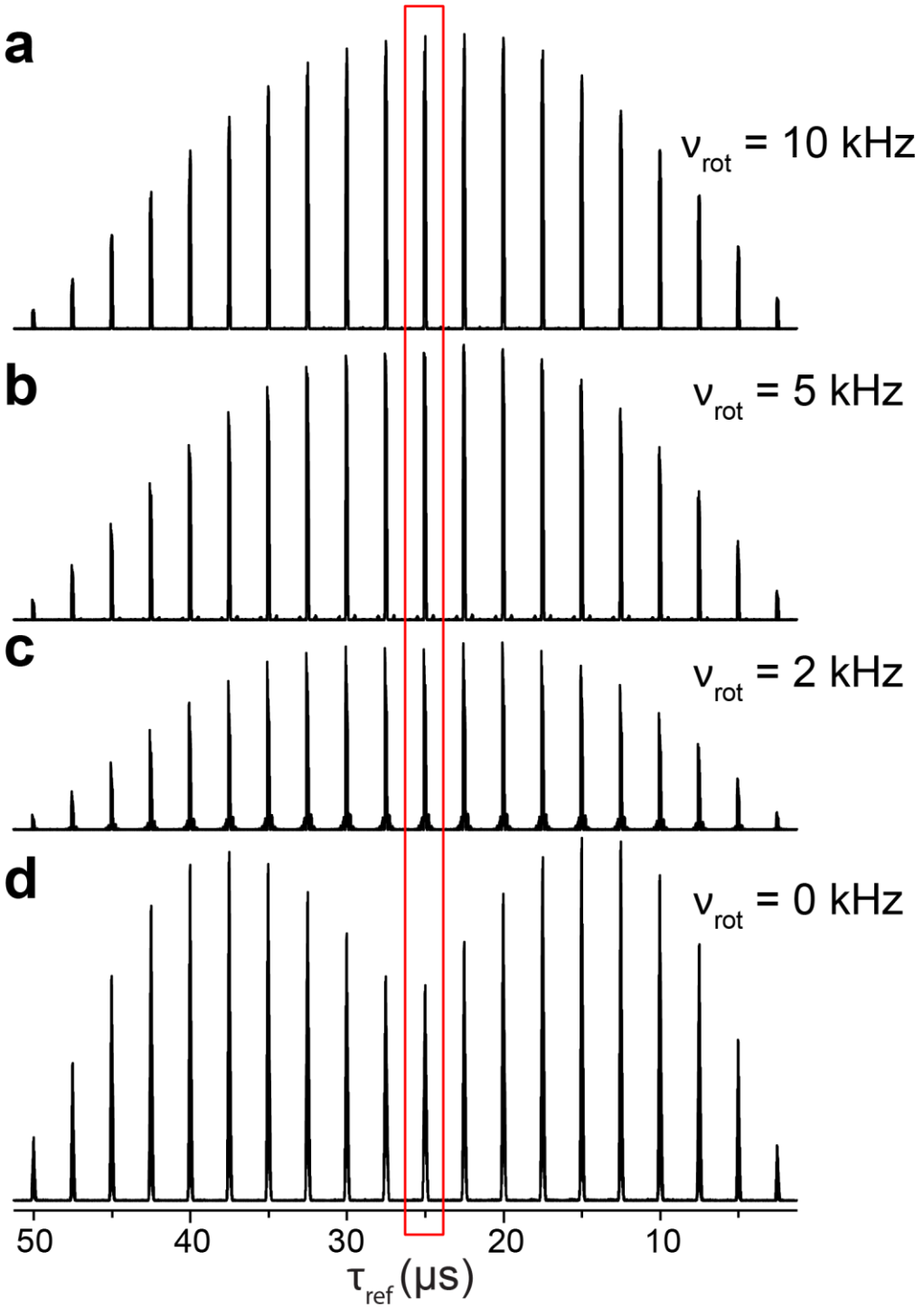

Figure S10 Experimental ^{87}Rb NMR spectra of $RbNO_3$ acquired with a CPMG pulse sequence using a RF amplitude of 10 kHz for all pulses, an excitation pulse width of 12.5 μs, and a refocusing pulse width (τ_{ref}) that is varied between 50 μs and 2.5 μs in 2.5 μs increments under (a-c) MAS and (d) static conditions. The red box indicates where a 25 μs refocusing pulse width is used and highlights the depletion of signal intensity if dipolar coupling is present. Spectra in each row are plotted on the same intensity scale but are not on the same intensity scale between rows.

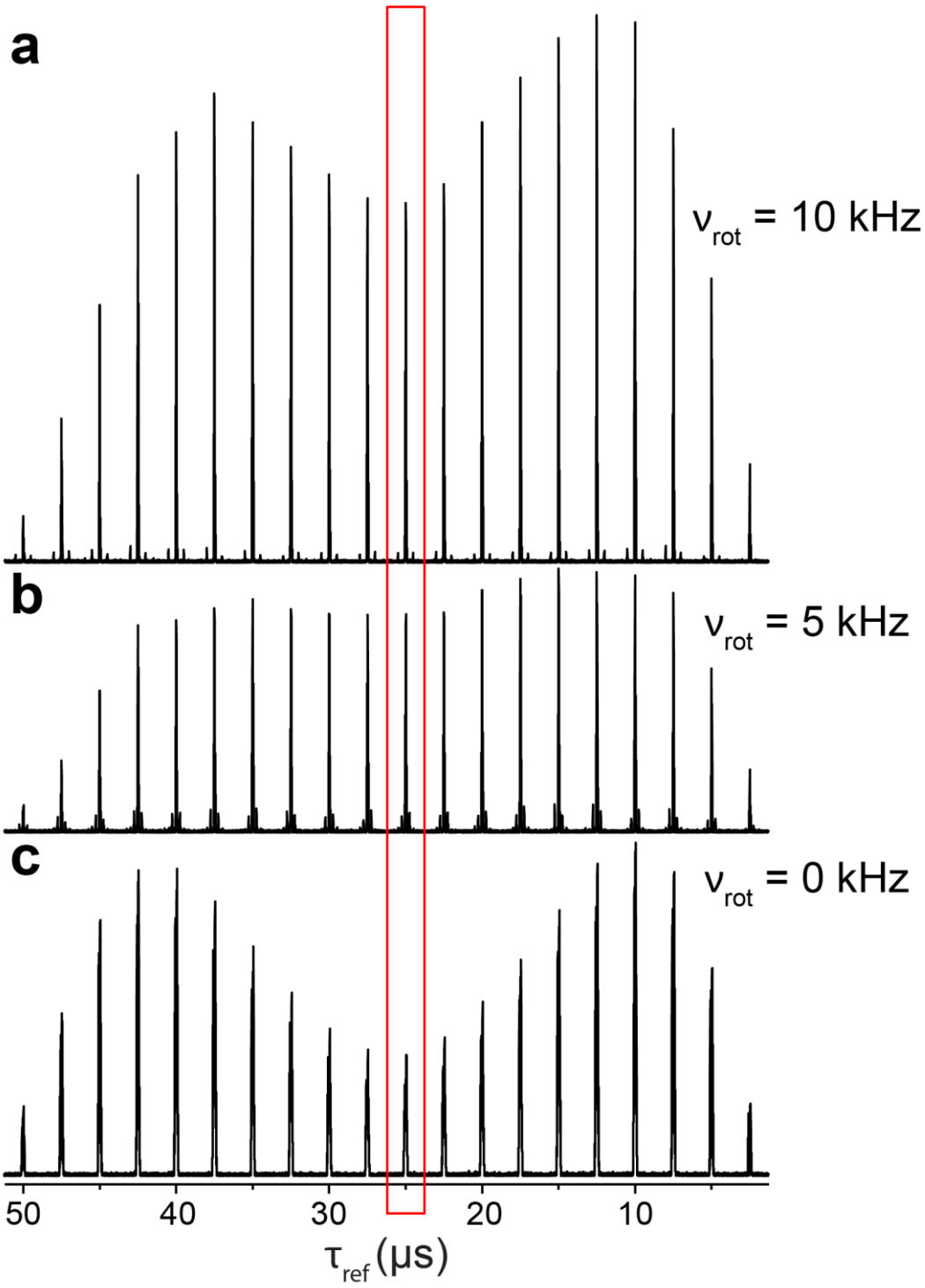

Figure S11: Experimental ^{23}Na NMR spectra of Na_2SO_4 acquired with a CPMG pulse sequence using a RF amplitude of 10 kHz for all pulses, an excitation pulse width of 12.5 μs, and a refocusing pulse width (τ_{ref}) that is varied between 50 μs and 2.5 μs in 2.5 μs increments under (a,b) MAS and (c) static conditions. The red box indicates where a 25 μs refocusing pulse width is used and highlights the depletion of signal intensity if dipolar coupling is present. Spectra in each row are plotted on the same intensity scale but are not on the same intensity scale between rows.

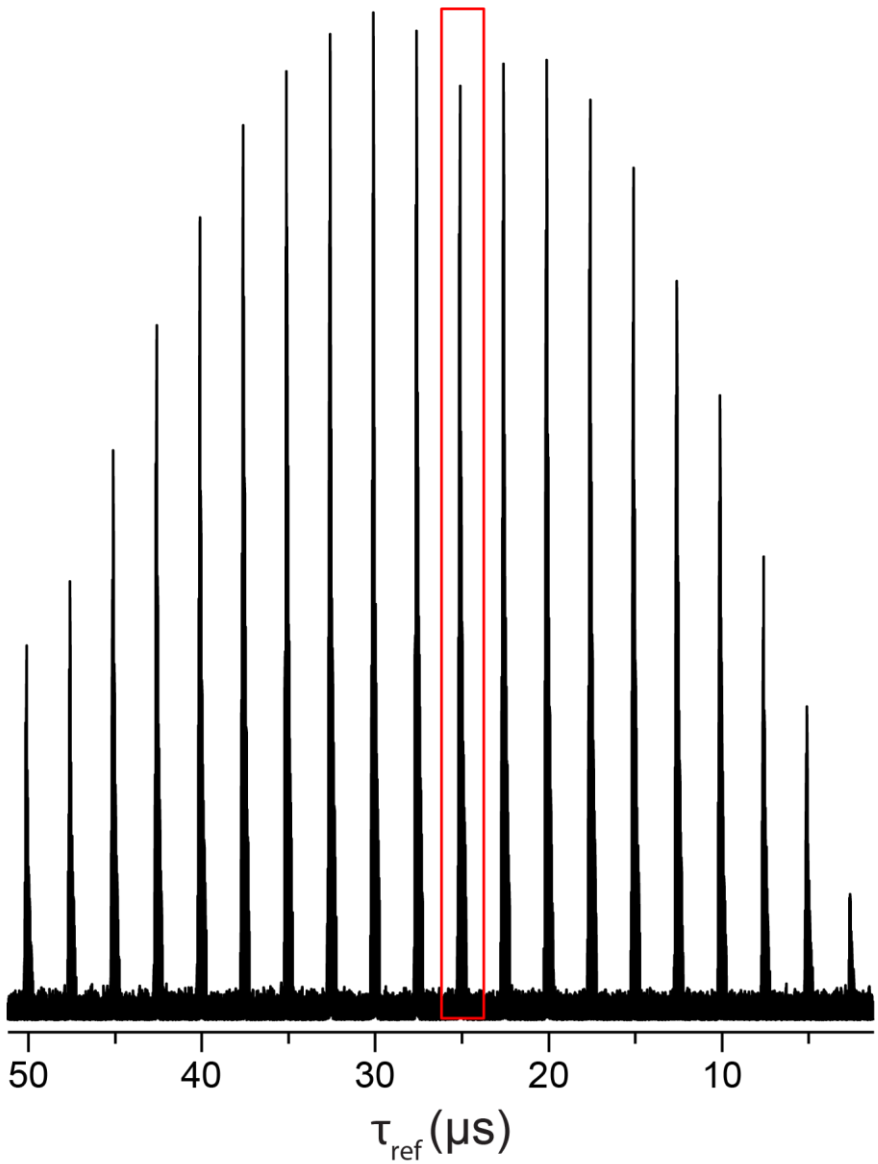

Figure S12: Experimental ^{35}Cl NMR spectra of L-histidine HCl·H_2O acquired with a CPMG pulse sequence using a RF amplitude of 10 kHz for all pulses, an excitation pulse width of 12.5 μs, and a refocusing pulse width (τ_{ref}) that is varied between 50 μs and 2.5 μs in 2.5 μs increments under static conditions. The red box indicates where a 25 μs refocusing pulse width is used and highlights the depletion of signal intensity if dipolar coupling is present. All spectra are plotted on the same intensity scale. It is noted that the array is lopsided likely from too short a relaxation delay between scans. The spectrum measured with τ_{ref} = 30 and 20 μs are in fact similar results, showing local maxima compared to the depletion at τ_{ref} = 25 μs, similar to the symmetric appearance shown in **Figure S3**, **S4**, and simulations in **Figure 11**.

References

(1) Iijima, T.; Nishimura, K. *Chem. Phys. Lett.* **2011**, *514*, 181–186.

(2) Iijima, T.; Shimizu, T.; Nishimura, K. *J. Magn. Reson.* **2015**, *251*, 57–64.

(3) Altenhof, A. R.; Jaroszewicz, M. J.; Lindquist, A. W.; Foster, L. D. D.; Veinberg, S. L.; Schurko, R. W. *J. Phys. Chem. C* **2020**, *124*, 14730–14744.

(4) Orendt, A. M.; Facelli, J. C.; Radziszewski, J. G.; Horton, W. J.; Grant, D. M.; Michl, J. *J. Am. Chem. Soc.* **1996**, *118*, 846–852.

Declaration of interests

☒The authors declare that they have no known competing financial interests or personal relationships that could have appeared to influence the work reported in this paper.

☐The authors declare the following financial interests/personal relationships which may be considered as potential competing interests: